The effect of subduction on the sulfur, carbon, and redox budget of lithospheric mantle

K.A. Evans[1] & Roger Powell[2]

[1] Dept. Applied Geology, Curtin University, GPO Box U1987, Bentley, WA 6845, Australia

[2] School Earth Sciences, The University of Melbourne, Vic 3010, Australia

Keywords: THERMOCALC, pyrite, magnetite, serpentine, oxidation

ABSTRACT

Subduction of hydrated lithospheric mantle introduces H_2O, ferric iron, oxidised carbon and sulfur to the subduction zone system. The fate of these components is poorly known but is intimately linked to the global geochemical cycles of iron, carbon and sulfur, the genesis of arc-related ore deposits, the temporal evolution of mantle redox state and subduction-related earthquakes and magmatism. THERMOCALC is used to provide first order constraints on the effect of subduction zone metamorphism on metamorphic redistribution of iron, carbon, sulfur and water in ultramafic rocks via construction of P-T and T-X(O) pseudosections with open system calculation of the effect of fluid loss.

The calculations replicate observed mineral assemblages in high pressure-low temperature ultramafic rocks at P-T conditions consistent with those suggested by other workers. The results are consistent with open system fluid loss without significant fluid infiltration. Water loss is complete by 850°C, the corresponding depth of fluid loss being consistent with that inferred for earthquakes in subducting slabs. Losses of carbon and sulfur are relatively minor, at around $< 5\%$ and $< 1\%$ respectively, so it is envisaged that most carbon and sulfur subducted in ultramafic lithologies is transported to > 5 GPa, below the depths of the source zone for arc volcanoes.

Oxygen activity for rocks in closed systems that evolve with a fixed redox budget is calculated to change from ΔFMQ -1 at 350°C to over ΔFMQ +3 at 850°C. This result emphasises the need to consider redox budget as well as oxygen activity when the results of experiments performed at fixed oxygen activity relative to some buffer are interpreted in the context of natural systems. In open systems, devolatilisation is calculated to increase the redox budget and oxygen activity of the residue via loss of methane and H_2S at the brucite-out and serpentine-out reactions respectively. No fluid-induced mechanism for oxidation of sub-arc mantle by transfer of redox budget from hydrated ultramafic lithologies to the overlying sub-arc mantle was identified, though further thermodynamic data on fluid species such as S_3^- are required to confirm this.

INTRODUCTION

Ultramafic rocks make up the lowest part of the lithosphere, the lithospheric mantle. The lithospheric mantle is effectively anhydrous and reacts with seawater at seafloor and sub-seafloor exposures. In recent years, reports of ultramafic rocks on the ocean floor at slow spreading ridges (Cannat *et al.*, 1997), transform faults (Dijkstra *et al.*, 2010), and continental margins (Beslier *et al.*, 2004) have increased the known extent of these rocks. Cannat *et al.* (2010) suggest that serpentinite makes up at least 9% of slow spreading basement by volume. In a more recent review of the serpentinite content of oceanic basement, Alt *et al.* (2013) estimated that serpentinites comprise 9–20% of slow spreading oceanic crust, and 2–5% of oceanic basement worldwide. Additional serpentinisation may occur at the lithospheric bend outboard of subduction zones (Ranero & Sallares, 2004). It has been proposed that serpentinisation at the slab bend may produce a layer several km thick and 10–20% serpentinised, so the global estimate of the proportion of serpentinites based on pre-subduction serpentinisation observations is a minimum.

Reaction with seawater involves oxidation and the addition of water, carbon dioxide, and sulfur (Mevel, 2003; Evans, 2012). Subduction of altered ultramafic rocks transports these added elements into the Earth's interior. Release of serpentine-hosted water at depths of 75–150 km is thought to provide significant water that aids mantle melting (e.g. Ulmer & Trommsdorff, 1995). The rheological consequences of subduction of hydrated ultramafic rocks are also significant. Serpentine-rich rocks are rheologically weak, and may play a key role in the geodynamics of subduction zones (e.g. Katayama *et al.*, 2009; Hirauchi *et al.*, 2010). However, the extent and consequences of subduction of relatively oxidised material involving ferric iron and oxidised forms of sulfur and carbon are much less well understood (but see Alt *et al.*, 2012b,a, 2013; Debret *et al.*, 2014b; Evans *et al.*, 2014; Giacometti *et al.*, 2014).

Slab-hosted iron, carbon and sulfur that are more oxidised than the iron, carbon and sulfur in the sub-arc mantle may be transported into the sub-arc mantle by metamorphic fluids produced by devolatilisation (Evans, 2012). Addition of these elements could change the redox budget of the sub-arc mantle. Redox budget is a compositional measure that quantifies the oxidising capacity of a material relative to a reference state. The redox

budget of a system is defined as the number of moles of electrons that need to be added to the system to reach a given reference state:

$$RB = \sum_i n_i \nu_i, \tag{1}$$

where RB is the redox budget, n_i is the number of moles of redox state i present in the sample of interest, and ν_i is the number of electrons required to take one mole of redox state i to the reference redox state (Evans, 2006).

Potential sources of redox budget for sub-arc mantle are of great interest because such sources may act to oxidise the sub-arc mantle (Kelley & Cottrell, 2009; Evans, 2006, 2012). An oxidised sub-arc mantle is required by some genetic models for the formation of arc-related ore deposits (e.g. Mungall, 2002; Sillitoe, 2010) but the extent to which sub-arc mantle is oxidised is controversial (Parkinson & Arculus, 1999; Lee *et al.*, 2005; Dauphas *et al.*, 2009; Mallmann & O'Neill, 2009; Kelley & Cottrell, 2009; Lee *et al.*, 2012; Evans, 2012).

The mobility of carbon and sulfur in subduction zones, regardless of their oxidation state, is also of interest. Sulfur is an important element in the formation of ore-deposits, but fundamental aspects of the fate of sulfur in subduction zones remain unknown (Alt *et al.*, 2012b,a, 2013; Debret *et al.*, 2014b; Evans *et al.*, 2014; Giacometti *et al.*, 2014). Subduction of carbonated lithologies is better studied; experimental evidence suggests that carbonate may remain stable in basaltic lithologies to high pressures (> 3.5 GPa) (Dasgupta *et al.*, 2004; Yaxley & Brey, 2004; Dasgupta *et al.*, 2005). If the same is true for ultramafic rocks then carbon added by subduction of altered lithospheric mantle may cycle carbon through the Earth's interior on timescales of 10s to 100s of millions of years.

Field observations and laboratory measurements that relate to redox budget in subducted ultramafic rocks allow a better understanding of the subduction cycling of iron, carbon and sulfur. However, interpretation of results from subducted rocks is hampered by the fact that these rocks have been exhumed, with associated retrogression, prior to examination. Exhumation commonly involves interaction with subduction zone and accretionary wedge fluids, and the effects of these fluid interactions can obscure prograde changes in mineral assemblage and mode that occur with subduction. Thermodynamic models of metamorphism of ultramafic rocks therefore provide a valuable complement to

studies of rocks.

Kerrick & Connolly (1998) used thermodynamic calculations to estimate the effect of subduction-related metamorphism on the CO_2 content of ultramafic rocks. These and subsequent workers (Fitzherbert *et al.*, 2004; Rüpke *et al.*, 2004; Sánchez-Vizcaíno *et al.*, 2005; Gorman *et al.*, 2006; Yang & Powell, 2006; Rebay *et al.*, 2012; Padrón-Navarta *et al.*, 2013) have demonstrated the utility and feasibility of thermodynamic modelling for ultramafic lithologies. However, this previous work has been restricted in a number of aspects. Then, it was not possible to properly describe the incorporation of ferric iron into minerals that are known to contain significant quantities of this element, such as serpentine and chlorite. Similarly, it was not possible to model sulfur-bearing phases at the same time as phases with complex activity-composition relations, like chlorite or even antigorite, until relatively recently (Evans, 2010). Further, the loss of redox-sensitive elements by devolatilisation requires the capacity for open system calculations, which was not available in conjunction with the other essential elements of the model.

Fortunately, recent developments in thermodynamic datasets, activity-composition relations, and thermodynamic modelling programs now allow simulation of ultramafic rocks to high pressures (5 GPa) in the system CaFMASCOSH (CaO–FeO–MgO–Al_2O_3–SiO_2–CO_2– O–S–H_2O) using the program THERMOCALC (Powell & Holland, 1988; Holland & Powell, 1998; Evans, 2010; Powell *et al.*, 2014; White *et al.*, 2014). In this work, a pseudosection-based approach is used to calculate phase assemblages, phase compositions and modes for serpentinised ultramafic bulk compositions under subduction conditions. The evolution of fluid composition during metamorphism is calculated, as is the distribution of redox budget between solid and fluid phases. Fluid can be gained or lost when rocks act as open systems, so knowledge of the fluid redox budget is central to the conclusions drawn here. The results of open system calculations are compared to those for closed systems to assess the effect of different fluid flow regimes on the evolution of mineral assemblages. Results are compared to observations of rocks from New Caledonia, China and the Western Alps. The results are used to provide theoretical constraints on the mobility of C and S, as well as on the overall redox budget evolution of subducted lithospheric mantle, and to infer conclusions for the evolution of the redox state of the deep mantle and sub-arc mantle wedge.

METHODS

Geological Setting

Samples that have undergone high pressure metamorphism in subduction zones were collected from the Pouébo terrane in New Caledonia, and the Zermatt Saas zone in the Western Alps. A brief geological background to both these areas is provided by Evans *et al.* (2014) and references therein. Samples from the Pouébo terrane were taken from the Mayanovitch creek exposures, which are described by Spandler *et al.* (2008), and from the Yambé ultramafic pod, which is described by Fitzherbert *et al.* (2004). Samples from the Zermatt-Saas were taken from the Lago di Cignana area, described by Reinecke (1991, 1998), and the Pfulwe area, which has been described by Barnicoat & Cartwright (1995); Fry & Barnicoat (1987); Dale *et al.* (2009). Thin sections were prepared and examined using a combination of transmission and reflected light microscopy with scanning electron microscopy (SEM). SEM was performed using a Hitachi TM3030 instrument with an Oxford instruments energy-dispersive X-ray (EDX) facility for recognition of fine-grained minerals. The accelerating voltage was 15 kV.

The bulk composition used in the pseudosection calculations was taken from an average of the composition of samples collected from the south-eastern exposures of the New Caledonian ophiolite. These samples have not undergone high pressure metamorphism, but are hydrated, with similar mineralogical features to those found in ocean floor exposures of ultramafic rocks (Evans, 2012), and are therefore considered to be an appropriate proxy for the protolith to the high pressure rocks. Bulk compositions of selected serpentinised harzburgites were measured by fusion in lithium tetraborate followed by dissolution and analysis by a combination of inductively coupled plasma mass spectroscopy (ICP-MS) and inductively coupled plasma atomic emission spectroscopy (ICP-AES). The ferrous iron content was obtained by titration with ceric sulfate, and the carbon and sulfur contents were obtained by combustion/infra-red methods on a LECO instrument. SY-4 was used as the standard for the ferrous iron analysis. All bulk composition analysis was undertaken at the Intertek Genalysis laboratories in Maddington, Perth. Full details of the bulk compositions are presented in Evans (2012).

The sulfur content of the average analysis used is 725 ppm S, which falls within the range of S reported from the volumetrically dominant high temperature serpentinites (320–2000 ppm S), and slightly lower than the S range from low temperature serpentites (850–2300 ppm S) (Alt *et al.*, 2013). The carbon content is 0.52 wt% C, which is at the high end of C contents for oceanic serpentinites (Alt *et al.*, 2013). Alt *et al.* (2013) report C contents of 0.18 to 1.7 wt% C in low temperature serpentinites, and 0.027–0.125 wt% in high temperature serpentinites. The effect of variations in C and S content on the consequences of subduction are discussed below.

Thermodynamic Modelling

Pseudosections and T-X sections were constructed using THERMOCALC v3.40i with dataset `tc-ds62.txt` of 6th Feb., 2012, henceforth `ds62` (Holland & Powell, 1998; Evans *et al.*, 2010; Holland & Powell, 2011) in the system CaO–FeO–MgO–Al_2O_3–SiO_2– CO_2–O–S–H_2O. Na_2O, K_2O, TiO_2 and MnO were not considered because the concentrations of these elements are commonly very low in ultramafic rocks. Fluids in the system CO_2–O–H_2O–H_2S can be considered, as has been possible since THERMOCALC 3.30i. A new feature in 3.40i allows fractionation of a phase during a sequence of calculation steps in temperature (or pressure). It is also possible to consider fluids that include solutes such as NaCl (Evans & Powell, 2006), but solutes were neglected for the purposes of this study.

Minerals considered were magnesite, dolomite, calcite, aragonite, orthopyroxene, clinopyroxene, olivine, brucite, antigorite, orthoamphibole, clinoamphibole, garnet, chlorite, talc, pyrite and pyrrhotite. The Mg serpentine end-member was assumed to have the thermodynamic properties of antigorite at all pressures and temperatures because temperatures considered were above the lizardite-antigorite transition (Ulmer & Trommsdorff, 1995; Wunder & Schreyer, 1997; Bromiley & Pawley, 2003; Evans, 2004; Schwartz *et al.*, 2013), and chrysotile is thought to be metastable (Evans, 2004). In `ds62`, in comparison with `ds60` (Holland & Powell, 2011), the incorporation of Al in antigorite to high P has been re-evaluated (*pers. comm.*, T. Holland). Activity-composition models used for silicate phases include new mixing models for antigorite and talc constructed using the micro-ϕ model of Powell *et al.* (2014) (*pers. comm.* G. Rebay). End-members for the

antigorite model are disordered Mg- and Fe-antigorite, an ordered Fe-Mg antigorite, an aluminous Tschermak-subsituted antigorite, and a ferri-Tschermak-substituted antigorite with ferric iron on the M1 site only. Calibration of the model involved adjustment of the DQF values of the ferrous and ferric antigorite end-members so that calculated serpentine–chlorite Fe-Mg partitioning matched those reported by Padrón-Navarta *et al.* (2010, 2011); Rebay *et al.* (2012) and Padrón-Navarta *et al.* (2013), and the ferric iron content matched those reported by Evans *et al.* (2012). The ferric iron dataset is limited in size and temperature resolution, so no attempt was made to incorporate temperature-dependence of ferric iron activity-composition relationships into the model.

Preliminary attempts to use the `ds62`-compatible activity composition models for chlorite and garnet of White *et al.* (2014) were made, but these models produced unrealistically high ferric iron contents in the calculated compositions of the minerals. Ferric iron was therefore neglected in garnet. Natural data suggest that the $Fe^{3+}/\sum$ Fe of mantle garnet is up to 0.1 (Berry *et al.*, 2010), but garnet does not become stable until the rock has lost most of its water and any accompanying C, S and redox budget, so the suboptimal nature of the garnet activity-composition relations is not a major issue for this work. Such an argument cannot be used for chlorite, so the DQF (Darken's Quadratic Formalism) parameter of the ferric iron end-member in chlorite was modified to give ferric iron values for chlorite co-existing with antigorite that match approximate values and partitioning calculated via charge balance constraints from the analyses in Rebay *et al.* (2012).

New amphibole and cpx activity-composition models for `ds62` are used (*pers. comm.* J. Diener, 2014), involving changes only to the DQF values from the models of Diener & Powell (2012). Ferric iron was not included in amphibole or clinopyroxene because its incorporation would normally be done via Na end-members, but the Na contents are very low in such rocks, and so Na has not been included in the system considered. The alternative incorporation of ferric iron by Tschermak's substitutions is not undertaken given the low reported Al content of pyroxenes and amphiboles, the compositions of which fall close to diopside and tremolite respectively (e.g. Rebay *et al.*, 2012; Bazylev *et al.*, 2013).

Details of the mixing model for pyrrhotite are provided by Evans *et al.* (2010). Pyrite

melts incongruently at 750°C at 1 bar to form a sulphur-rich liquid and pyrrhotite (Toulmin & Barton, 1964). The melting point will increase with pressure because the volume change of the melting reaction is positive, so sulphide melts will, most likely, not form in the modelled system at the temperatures of interest. It was therefore possible to exclude sulphide melts from the model.

The model for dolomite was taken from White *et al.* (2003) with adjustments of the DQF for ferroan dolomite to produce calculated partitioning between dolomite and chlorite consistent with observations in natural systems. The magnesian carbonate solid solution was modelled with a symmetric formalism approach (Holland & Powell, 1996), with a small DQF on the ferroan end-member calibrated against the data of Rosenberg (1967).

There is not yet an orthoamphibole model for `ds62` (*pers. comm.* J. Diener). This means that calculated phase relations in the *PT* range where anthophyllite is likely to be stable (e.g. > 500°C at 0.3–0.5 GPa (Barnes *et al.*, 2009)) may be metastable with respect to orthoamphibole. This is not a concern as mineral stabilities at these pressures and temperatures are not of major interest for this study.

The maximum pressure investigated is 5 GPa. Equations of state for H_2O and CO_2 in THERMOCALC are those of Pitzer & Sterner (1994), and are robust to 10 GPa. Mixing of H_2O and CO_2 was calibrated on data from pressures to 2 GPa, so calculations to 5 GPa involve extrapolation. However there are no critical points or phase changes in the *P-T* range over which the model is extrapolated so extrapolation to 5 GPa can be made with a moderate degree of confidence. However, as with all extrapolations, results must be treated with caution and data to test the model should be sought.

A pressure-temperature pseudosection was constructed to allow the pressure- and temperature-sensitivity of the mineral assemblages to be assessed (Fig. 1). The H_2O content of this bulk composition was adjusted so that olivine could be completely replaced by brucite and serpentine at low temperatures to simulate metamorphism of a fully serpentinised protolith. The composition for components other than water was taken from the average of the ultramafic rocks analysed for this study (Table 1).

The initial modelling mimics a fluid-saturated closed system, from which fluid cannot escape during heating, although the fluid composition can change as a result of the

formation and devolatilisation of H_2O-, CO_2-, and S-bearing minerals. This conceptual model does not match physical reality, where evolved volatiles are likely to be lost from the system. However, the model provides a convenient reference calculation with which the open system calculations can be compared. Care must be taken if the pressure-temperature path followed requires substantial rehydration (Guiraud *et al.*, 2001; Clarke *et al.*, 2006). In this case, the water required for hydration reactions to go to completion is in excess of that present in the starting composition. Under these circumstances, the starting proportion of H_2O in the bulk composition can have a strong influence on the predicted mineral assemblages. However, preliminary calculations confirmed that pressure and temperature increases on all of the geotherms investigated lead to progressive fluid loss, that fluid is present at all times, and that the availability of fluid does not limit the range of possible mineral assemblages.

Mineral modes and fluid compositions for lithospheric mantle were calculated up to 5 GPa along hot and cold geotherms of van Keken *et al.* (2002), modified to be linear in P-T space to facilitate the calculations (Figs 2 & 3). The hot geotherm is for slowly converging (2 cm year^{-1}) relatively young 20 Ma crust with a steep slab dip of 60^o; the cold geotherm is for rapidly converging (10 cm year^{-1}), 100 Ma old crust with a slab dip of 30^o. The distribution of redox budget between the different mineral hosts and fluid were also calculated. These calculations allow a first order assessment of the potential of devolatilised fluids to oxidise the mantle wedge. All modes are normalised on a one-element basis, so, for example, the mode of quartz on a one element basis in a quartz-magnetite rock would be $\frac{3m_{\mathrm{SiO_2}}}{3m_{\mathrm{SiO_2}}+7m_{\mathrm{Fe_3O_4}}}$, where m_k is the number of moles of k, and where k represents the mineral of interest, e.g. SiO_2 to represent quartz.

The sensitivity of assemblage evolution to initial redox budget was calculated with a T-X_{O} section calculated at 2.6 GPa (Fig. 4). X_{O}, the proportion of the component O in the set of oxide components, is equivalent to the redox budget of the system for a reference state of Fe as FeO, S as SO_2, and C as CO_2. Using this reference state, X_{O} is equal to $\frac{1}{2}\,\mathrm{Fe}^{3+} - \frac{5}{2}\,\mathrm{S}^{-} - 3\,\mathrm{S}^{2-} - 4\,\mathrm{C}^{4-} - 2\,\mathrm{C}^{0}$. A negative X_{O} is possible because S is present as either S^- in pyrite, or S^{2-} in pyrrhotite or H_2S, rather than as SO_2, and this is the case here for most reasonable S contents. X_{O} was varied sufficiently to allow stabilisation of a range of redox-sensitive phases such as magnetite, hematite, pyrite and pyrrhotite. This

range of redox budgets and assemblages covers the range of assemblages observed in altered lithospheric mantle. The purpose of these calculations is to allow the effect of initial redox budget on phase stability and devolatilisation to be considered, albeit with the simplification of constant pressure. The figure was contoured for oxygen activity relative to the FMQ (fayalite-magnetite- quartz) redox buffer, to allow the relationship between the extensive and intensive redox variables, redox budget and oxygen activity, to be investigated (Fig. 4).

Open system processes were investigated at a fixed pressure of 2.4 GPa (Figs 5 & 6). An isobaric P-T path at this pressure crosses most of the fields seen by rocks on either the hot or cold geotherms investigated here. Most of the mineral isopleths are close to vertical in $P-T$ space, so the lack of opportunity to vary pressure during this calculation is not considered to reduce the utility of the calculations significantly. Temperature steps were 5°C in the quadrivariant and quinivariant fields, where fluid production was low, but decreased to 1°C or 0.1°C in the trivariant and divariant fields where fluid production was more voluminous. The temperature step was chosen so that the fluid produced in any given step was less than 1% mode (all modes on a one element basis), with the fluid content in the rock being reduced to 1% mode at each temperature step, if necessary. The value of 1% is higher than that expected in metamorphosing rock at high pressure, however, it has the advantage of ease of calculation and enables comparison of the first order differences between closed and open systems, which is a major aim of the exercise. The fluid considered is H_2O-CO_2-H_2S-CH_4 at lower temperatures, and H_2O-CO_2-H_2S at temperatures above the brucite–olivine transition at about 500°C, where the proportion of methane became negligible in these calculations. SO_2 was not included because we don't have good data for this fluid species, and because there is no evidence that SO_2 occurs in significant concentrations in subduction zone fluids at the pressures and temperatures of interest. The iron oxide phase considered had the composition of magnetite throughout. Mineral modes, fluid compositions and redox budget contributions (Figs 5 & 6) were calculated and compared to closed system modes, fluid compositions and redox budgets on the same isobaric path (Fig. 7).

RESULTS

P-T section

The pressure-temperature pseudosection, (Fig. 1), is similar, in terms of the major phase changes, to those calculated for simpler systems (e.g. Kerrick & Connolly, 1998; Yang & Powell, 2006; Rebay *et al.*, 2012; Padrón-Navarta *et al.*, 2013; Scambelluri *et al.*, 2014) and assemblages are also consistent with those observed in ultramafic rocks from other metamorphic settings (e.g. Gole *et al.*, 1987; Barnes *et al.*, 2009). Reactions involving the major silicate phases are the conversion of brucite to olivine at 425–500°C, introduction of talc and/or orthopyroxene depending on pressure at around 600°C, growth of chlorite at the expense of antigorite at around 650°C, the loss of chlorite at 750–800°C and growth of garnet at high pressures (> 2.7 GPa) and temperatures (> 750°C).

The stability fields of the Ca-bearing phases, dolomite, diopsidic clinopyroxene, and tremolitic amphibole, intersect at around 625°C and 1.8 GPa. Dolomite is stable in the low $P-T$ part of the diagram, amphibole at lower pressures and higher temperatures, and clinopyroxene at high pressure and the full range of temperature. Magnesite is stable over a wide range of pressure, to 5 GPa, and temperature, but is lost as temperature increases at lower pressures (< 2 GPa). Magnesite is stable with dolomite, antigorite, pyrrhotite, magnetite and brucite at the lowest temperatures and pressures examined (< 450 to 500°C and 2.5 GPa).

The stable sulphide phase is pyrrhotite at lower temperatures and pressures (< 580 °C and 2.7 GPa) and pyrite otherwise. This prediction is initially surprising because pyrite is stable at lower temperature and pyrrhotite at higher temperature in most mafic and pelitic rock compositions (e.g. Ferry, 1981), and is discussed further below.

Modes and phase compositions on the hot and cold geotherms

Mineral modes on the hot and cold geotherms are broadly similar (Figs 2a-c and 3a-c). On the hot geotherm, antigorite drops from a mode of around 0.85 to about 0.65 when olivine

replaces brucite, and then drops to zero as orthopyroxene and chlorite-forming reactions proceed to completion. Identical reactions occur on the cold geotherm, although the lower temperature phases occupy a greater proportion of the $P-T$ path on the cold geotherm. The brucite mode increases from around 0.04 to about 0.055 during the early part of the $P-T$ path but drops to zero at just below 500°C. Chlorite grows at the expense of antigorite at around 600°C, but is never present in large quantities, with a maximum mode of about 0.02, because of the Al-poor nature of the bulk composition. Garnet is present at the highest temperatures on the hot geotherm only, the cold geotherm does not reach the garnet-stable fields at pressures less than 5 GPa. Talc is not stable on either geotherm. Magnetite is stable on both geotherms, and in both cases exhibits a minimum in mode at intermediate temperatures, with the minimum much more pronounced on the hot geotherm. The magnetite mode drops by õne third on the cold geotherm, and by $\tilde{8}0\%$ on the hot geotherm, though the magnetite mode is initially much higher on the hot geotherm because of the presence of methane in the fluid (see below).

Pyrite replaces pyrrhotite at 430 °C, on the cold geotherm and at around 570 °C on the hot geotherm (Fig. 2c and 3c). The conversion from pyrrhotite to pyrite does not cause any significant change in the concentration of H_2S in the fluid (Fig. 2d and 3d). Total integrated fluid production is similar on both geotherms, in spite of the lower temperatures reached on the cold geotherm by 5 GPa. The similar fluid production reflects that the bulk of fluid is produced at the brucite to olivine reaction at around 500 °C, and at the antigorite to orthopyroxene + chlorite + olivine reaction at around 600 °C. Both of these reactions are completed by 5 GPa, regardless of geotherm.

The fluid composition is dominated by H_2O. The low solubility of CO_2, CH_4 and H_2S means that these species form less than 5% of the fluid phase at all temperatures, with lower solubilities on the cold geotherm (Fig. 2d and 3d). Methane is calculated to be present in significant quantities in the fluid only on the hot geotherm at temperatures less than 520 °C, and its proportion drops to zero during the brucite to olivine reaction (Fig. 2d, 3d). Methane is not shown on Fig. 3d because its concentration in the fluid is negligible.

The presence of methane below 500 °C, though at mole proportions in the fluid phase less than 0.03, has a significant effect on the redox budget of the solid phases on the hot

geotherm (Fig. 2e). The redox budget of methane is negative, so production of methane increases the redox budget of the solid residue. When CH_4 converts to CO_2 with increasing temperature, there is an accompanying decrease in the redox budget hosted by the solid phases (Fig. 2f). This decrease is accommodated mostly by a drop in the magnetite mode (Fig. 2e). Magnetite hosts the bulk of the redox budget below about 560 °C, at which point pyrite becomes stable. At temperatures higher than 560 °C, magnetite and pyrite hold about 50% of the redox budget each. Methane is not present in significant quantities in the fluid produced on the cold geotherm, and this is the reason for the less pronounced minima in magnetite mode on the cold geotherm (Fig. 3e).

The silicate phases, chlorite and antigorite, hold only a small fraction of the redox budget (Fig. 2e and 3e). This is reflected in the small but significant fraction of ferric iron predicted for these phases (Fig. 3f). The concentration of ferric iron in chlorite is twice as high as that in antigorite, but the modes of chlorite are low compared to those of antigorite, so the total amount of ferric iron held by antigorite is greater than that held by chlorite.

Sensitivity of assemblage to redox budget

Redox-sensitive mineral phases predicted to be stable as a function of redox budget, X_O, vary from pyrrhotite-only at the lowest redox budgets and temperatures to pyrite and hematite at the highest redox budgets and temperatures (Fig. 4). Anhydrite was not calculated to be stable in the range of conditions modelled. Magnetite is stable at intermediate redox budgets at all temperatures. At lower temperatures the sequence of redox-sensitive phases with increasing redox budget is pyrrhotite, pyrrhotite + magnetite, pyrrhotite + pyrite + magnetite, pyrite + magnetite and pyrite + hematite + magnetite. At about 570 °C this sequence shifts, via the termination of the pyrrhotite-pyrite-magnetite trivariant field, to pyrrhotite, pyrrhotite + pyrite, pyrite, pyrite + magnetite, pyrite + magnetite + hematite and pyrite + hematite. The boundaries between pyrrhotite and pyrite, and between magnetite and hematite, both follow an approximately S-shaped pattern across the diagram.

Contours of $\log_{10} a_{O_2}$ relative to the hypothetical FMQ (fayalite-magnetite-quartz) buffer follow a similar S-shaped pattern (Fig. 4). The contoured value is ΔFMQ, which is

defined as $\log_{10} a_{O_2}$ - $\log_{10} a_{O_2}^{FMQ}$. The lowest ΔFMQ values, around -2, are associated with the most reduced assemblages at the lowest temperatures, while the highest ΔFMQ values, of up to +5, are associated with the most oxidised assemblages at the highest temperatures. Increasing temperature at constant X_O leads to an increase in ΔFMQ of several log units. For example, a sample with an initial X_O of -0.14, similar to that of the sample modelled in the other figures, starts at 350 °C with a ΔFMQ close to -1, consistent with what is known about hydrated oceanic lithosphere. The opaque phase assemblage at 350 °C is pyrrhotite-magnetite, but the pyrite–magnetite field projects to lower X_O as T decreases, so the predicted opaque assemblage at less than about 300°C is pyrite–magnetite, consistent with observations (e.g. Alt *et al.*, 2013). If this rock undergoes an increase in temperature without any change in X_O then, by 850 °C, ΔFMQ increases to over +3, an increase in over 4 log units. This increase is not accompanied by any significant oxidation of the rock, but simply by a change in the distribution of the electrons, and a change in the availability of those electrons for subsequent reactions.

Open system calculations

Loss of fluid during the open system calculations led, unsurprisingly, to significant reduction of the water content of the original bulk composition, from 28 mole% at 350°C to zero mole% held in the solid phase at 850 °C (Fig. 5a). The bulk of fluid loss occurs during the transformation of brucite to olivine at around 500°C, and the transformation of antigorite to chlorite at 625 to 650°C. These significant losses of water were not accompanied by significant changes in the CO_2 or SO_2 content (Fig. 5b,c). CO_2 changes by less than 5% and only about 1% of the sulphur is lost as temperature increases from 350 °C to 850 °C because the solubility of both CO_2 and H_2S in the devolatilised fluid is low.

Changes in the modes of most phases and the evolution of fluid composition parameters are similar to those in the closed systems on identical PT paths (compare Figs 7a to d with Figs 6a to d). The temperatures of phase field boundaries for the open and closed system calculations are identical to within 1 or 2°C, and the sequence of mineral assemblages is also identical.

Important aspects that differ between the open and closed systems are the magnetite

mode (compare Fig. 6C and Fig. 7c) and redox budget (Fig. 6e and Fig. 7e). In the closed system, magnetite shows an overall decrease in mode with progressive metamorphism and is only about 40% of that in the open system at temperatures above that of the brucite-to-olivine reaction. Magnetite in the open system shows an overall increase with increasing temperature; this increase is related to the loss of reduced species in the fluid phase and consequent increases in the solid phase redox budget.

The solid phase redox budget climbs by about a third as temperature increases from 350 °C to 850 °C. This redox budget increase occurs in two distinct steps, one at around 530 °C, and the second around 650 °C. The first step is associated with the loss of methane at the brucite to olivine reaction discussed above. The second step is associated with the loss of H_2S during antigorite breakdown. This increase in redox budget is accommodated by increases in the magnetite and pyrite modes, and, to a lesser extent, by ferric iron in antigorite. Changes in redox budget can affect the stable phase assemblage (Fig. 4). For the modelled system, the increase in redox budget predicted for the open system model produces identical final assemblages for the open and closed systems, and a change in only a few tenths of a log unit in ΔFMQ. However, it can be seen that there are locations on Fig. 4 where relatively small changes in redox budget could have a significant effect on ΔFMQ.

DISCUSSION AND CONCLUSIONS

Comparison with rocks

Alpine Examples

The petrology of high pressure rocks from the Zermatt-Saas zone of the Western Alps is described by Rebay *et al.* (2012). The eclogite facies assemblage of the ultramafic samples studied is antigorite + olivine + clinopyroxene + chlorite (Fig. 8a). The inferred temperature is above 600°C at a pressure greater than 2.5 GPa. The opaque components of the mineral assemblage are not described by Rebay *et al.* (2012), though examination of thin sections of partially retrogressed rocks from this area (grid refs: WGS 84, zone 32T,

391613 mE and 5080719 mN) reveals the presence of small, rare pyrite (Fig. 8b) and chalcopyrite grains (Fig. 8c), and common Ti-rich magnetite, Ti-poor magnetite, Cr-rich magnetite, and ilmenite. Large euhedral magnetite grains are rimmed by talc (Fig. 8d), and intergrown with late chlorite (Fig. 8e). The proportion of sulphur-bearing phases is less than 1%.

The assemblage in the Zermatt Saas samples studied, apart from Cu-, Ti- and Cr-bearing minerals, which are not modelled, is consistent with the calculated assemblage illustrated in field Z of Fig. 1, except for the presence of chlorite in the rocks, and the absence of carbonate. The temperature range over which chlorite is stable is expected to vary as a function of bulk composition, particularly the Al-content, because Al stabilises chlorite. The bulk composition used in these calculations is relatively Al-poor; higher Al-contents stabilise chlorite at lower temperatures than those seen here. Thus the presence of chlorite in the more aluminous Zermatt Saas section is unsurprising. Another factor that must be taken into account is that the composition of chlorite that co-exists with serpentine in ultramafic rocks is likely to be more complex than that of the ideal chemical formula used here. Interlayered chlorite-serpentine minerals from the Lizard ophiolite complex and from Lancaster County, Pennsylvania, have been described (Banfield & Bailey, 1996; Cressey *et al.*, 2008). Preliminary work on rocks from the Western Alps suggests that these complex interstratified chlorite-serpentine minerals may be present here. It is therefore acknowledged that further work on chlorite and serpentine characterisation and activity-composition relationships is required before chlorite and serpentine relationships can be understood and interpreted with confidence. Late talc on magnetite is interpreted to record decompression, because the maximum pressure for talc stability is around 1.5 GPa. The absence of carbonate in the natural samples contrasts with the widespread predicted stability of magnesite. The preferred reason for magnesite absence in rocks is the lower C content of the Zermatt Saas bulk composition compared to the modelled bulk composition, which lies at the higher end of C contents in serpentinised peridotite (Alt *et al.*, 2013). The implications of variation in C contents for subduction cycling of C are discussed below.

New Caledonia

Fitzherbert *et al.* (2004) and Spandler *et al.* (2008) describe ultramafic rocks from north-east New Caledonia. These rocks occur as metre to decimetrescale pods interleaved with high pressure eclogite and blueschist facies metabasites with peak inferred pressures around 2 GPa and 590°C. The pods are surrounded by a blackwall assemblage of talc, magnesite, tremolite, chlorite plus accessories that include apatite, rutile and titanite. The peak mineral assemblage within the pods is olivine, antigorite and Cr-spinel, with early magnetite and late retrogession-related talc and brucite. The opaque components of the assemblage are not described in detail. However, examination of thin sections from this area (grid refs: WGS 84, Zone 58K 0435903 mE 7758738 mN) reveals the presence of complex compositional variation in magnetite-spinel minerals, including concentric zoning in magnetite included in magnesite (Fig. 8f), Ti-poor rims with Ti-rich exsolution lamellae and flame-like hematite exsolution structures (Fig. 8g). Additionally, magnetite is associated with late carbonate-chlorite-bearing veins (Fig. 8h).

The peak assemblage, like that of the Zermatt Saas samples, is closest to that of the field marked Z on Fig. 1. The absence of a Ca-bearing phase and pyrite is likely to be due to low Ca and S respectively in the bulk composition. The talc-carbonate blackwall assemblages that rim the serpentinite pods have clearly experienced metasomatic bulk composition changes (Spandler *et al.*, 2008) which would require additional work to simulate. However, a preliminary interpretation, based on that of Spandler *et al.* (2008), is that formation of carbonate minerals driven by addition of CO_2 effectively decreased the cation:Si ratio available for silicate minerals and stabilised talc.

Northern Quaidam Mountains, North West China

Yang & Powell (2006) describe the petrology of UHP garnet peridotites from the Northern Quaidam Mountains (NQM), China. These rocks are associated with serpentinites and a range of non-ultramafic lithologies that include gneisses, granites, migmatites, metabasites and metasedimentary units. The assemblage interpreted as peak in the least altered garnet lherzolite samples is olivine, garnet, orthopyroxene and clinopyroxene (± cummingtonite ±

phlogopite). Peak pressure-temperature conditions are estimated to be 3.0–3.5 GPa and around 700°C. The peak assemblage is consistent with the calculated assemblage in field Q of Fig 1, except for the absence of magnetite in the natural assemblage, which can be attributed to a lower redox budget in the NQM samples compared to the modelled sample, the lack of carbonate, which is attributed to lower C in the rock than in the modelled bulk composition, and the attribution of observed chlorite to retrogression (Yang & Powell, 2006), whereas chlorite could have been stable at the peak conditions. Minerals interpreted to be associated with retrogression by Yang & Powell (2006) include talc, antigorite, pargasite, chlorite and magnetite. The growth of all of these minerals except for chlorite is consistent with a decrease in pressure and temperature during retrogression, although chlorite may have been stable even at temperatures as high as 700 °C, according to Fig. 1. However, as stated previously, further work is necessary before the precise pressures and temperatures of chlorite stability can be calculated with confidence.

Summary of comparison with rocks

Pseudosections are only strictly valid for the specific bulk composition modelled but Fig. 1 replicates mineral assemblages found in the selected high pressure ultramafic rocks well, so long as the likely effects of variations in bulk Al-, C- and S-content are taken into account. The chosen bulk composition has lower S than the S concentration in low temperature serpentinites, and higher C than the average of oceanic lithosphere serpentinites reviewed by Alt *et al.* (2013). If the bulk composition had lower S, then the mode of sulphides would be less, but changes to the average value of Alt *et al.* (2013) would not alter the position of boundaries between assemblages or the sequence of assemblages significantly. If the bulk composition had lower C, then the mode of carbonate would be lower, and C in the rock could be exhausted by loss of CO_2. Indeed, the lack of carbonate in two of the three localities is consistent with C contents in the protolith lower than those used in the modelling.

The least successful aspect of the modelling relates to chlorite and antigorite, which may be due to the presence of interstratified chlorite-antigorite phases, as well as to a lack of data for Al-poor chlorites. If higher geothermal gradients were to be considered then the

lack of magnetite-spinel solid solutions could prove problematic. Additionally, trace elements such as Ti and Ni may stabilise phases such as ilmenite, which is observed in specimens from the Zermatt-Saas (Li *et al.*, 2004), and pentlandite, which is observed in other ultramafic localities (e.g. Alt *et al.*, 2012a; Shimizu *et al.*, 2013; Scambelluri *et al.*, 2014, see discussion below).

Relative stability of sulphide phases

The predicted conversion of pyrrhotite to pyrite with increasing temperature, rather than pyrite to pyrrhotite, as is the case in pelitic rocks and during simple system experiments (Toulmin & Barton, 1964; Ferry, 1981), is initially surprising and requires further discussion. In ultramafic rocks, the minerals that dominate at low temperature, such as serpentine and brucite, contain little Fe, so Fe is held in magnetite and iron-bearing alloy phases (e.g. Evans, 2008; Frost *et al.*, 2013). The relative abundance of available Fe at lower temperatures stabilises pyrrhotite over pyrite. At higher temperatures, more Fe-rich silicate phases are stabilised, availability of Fe relative to sulphur decreases, and pyrite becomes the most stable phase if Fe and S are not very mobile. This relative availability of Fe contrasts with that in mafic and pelitic compositions, where increasing temperature increases X_{Mg} in minerals, and thus favours formation of Fe-rich accessory minerals. This interpretation and the calculated results are also consistent with the results of Frost (1985), who noted that carbonate-poor ultramafic rocks contain sulphur-poor sulphides such as heazlewoodite and pyrrhotite, whereas carbonate- and talc-bearing ultramafic rocks contain the sulphur-rich sulphide, pyrite. In this case, the presence of carbonate can be considered to decrease the availability of cations for sulphide phases, so that, in the absence of other factors, the highest cation:sulphur ratios occur when carbonate is absent, and the lowest cation:sulphur ratios when carbonate is present in significant quantities.

The relative stability of pyrrhotite and pyrite can also be related to oxygen activity, with pyrrhotite stable at lower $a_{\mathrm{O_2}}$ values than pyrite. The 'S' shaped ΔFMQ isopleths in Fig. 4 confirm that ΔFMQ increases with temperature without any change in the redox budget of the rock, and that, therefore, pyrrhotite converts to pyrite for a wide range of bulk compositions investigated. This is potentially an important result of this work,

because the observation of a change from stable pyrite to stable pyrrhotite in natural systems is commonly taken to indicate that a rock has, in some way, been reduced, possibly by infiltration of a reducing fluid (e.g. Neumayr *et al.*, 2008; Evans, 2010). However, in rock-dominated systems a_{O_2} is controlled by the rock (Evans *et al.*, 2013; Frost *et al.*, 2013) so it is likely that the presence of pyrrhotite is a record and consequence of rock buffered a_{O_2}, rather than a record of the infiltration of reduced fluids.

Pyrite was observed in the rocks examined in detail for this study (see above). However, coexisting pyrrhotite, pentlandite and magnetite have been reported from high pressure - low temperature localities such as Cerro del Almirez, Erro Tobbio, and Cima di Gagnone (e.g. Alt *et al.*, 2012a; Shimizu *et al.*, 2013; Scambelluri *et al.*, 2014). All these rocks would have reached peak conditions in the pyrite-stable regions of Fig. 1, although in most cases the temperatures would have been higher than on the slab geotherms shown in Fig. 1. A number of factors may have affected the stable sulphide. These include: a lower redox budget for the protolith than that modelled; a geodynamic setting that allowed fluid infiltration that changed the redox budget and stabilised pyrrhotite; and stabilisation of pyrrhotite by mixing with a Ni-bearing end-member, which is not included in the model used. Shimizu *et al.* (2013) and Scambelluri *et al.* (2014) propose a mantle wedge and a slab-wedge interface setting for the Erro Tobbio and Cima di Gagnone ultramafic rocks respectively, and possible fluid flow regimes for these environments are discussed below.

Devolatilisation and loss of C, S, and redox budget

Water

Subducted peridotite undergoes two main episodes of water loss. The first, associated with conversion of brucite to olivine, results in about one third of the overall water loss, with negligible losses of CO_2 and sulphur. The brucite to olivine reaction occurs at around 1.5 GPa and 490 °C on the hot geotherm and 4.5 GPa and 530 °C on the cold geotherm. The second main fluid release episode is associated with breakdown of antigorite to orthopyroxene, olivine, and chlorite at 2.4 to 2.6 GPa and 630 to 660 °C on the hot geotherm, and and 4.6 to 4.7 GPa and 560 to 570 °C on the cold geotherm. The difference

between the temperatures of the two dehydration reactions is about 40°C on the cold geotherm and about 140°C on the hot geotherm. The pressure difference, however, is not so significant, so the spatial difference between the depths of water release is likely to be similar on a wide range of geotherms.

The calculated pressures for the fluid release episodes are somewhat lower than those calculated by Gorman *et al.* (2006) using older datasets and activity-composition models. These workers inferred from model results that upper oceanic mantle dehydration would not occur at pressures above 5 GPa on cooler geotherms, and was therefore considered an insignificant source of fluid to drive CO_2 decarbonation in overlying mafic crust within the slab at sub-arc depths. Similarly, Gorman *et al.* (2006) considered that dehydration of upper oceanic mantle on hot geotherms occurred at depths too shallow to affect arc magmatism; these statements are discussed further below.

Carbon

Less than 5% of the original carbon is predicted to be lost during prograde metamorphism of the bulk compositions studied here. CO_2 is predicted to be relatively insoluble in the fluids released by the rocks, with X_{CO_2} always less than 0.03 at temperatures less than 800°C (Figs 2d, 3d, 6d). X_{CO_2} is predicted to be highest at the highest temperatures in the open system calculations (Fig. 6d). Thus, if the calculated CO_2 solubilities are correct then the bulk of CO_2 subducted in ultramafic rocks is likely to be transported to depths greater than 150 km. This result is consistent with those of previous experimental studies (e.g. Dasgupta *et al.*, 2004; Yaxley & Brey, 2004; Dasgupta *et al.*, 2005), and with observations of rocks (Alt *et al.*, 2012a,b, 2013). Voltri Massif antigorite serpentinites have the same carbon contents as lower grade lizardite-bearing serpentinites in the Apennine ophiolite, suggesting that the lizardite–antigorite transition does not drive carbon loss (Alt *et al.*, 2012b). Similarly, antigorite serpentinites and olivine–orthopyroxene–chlorite harzburgites at Cerro del Almirez also have statistically indistinguishable carbon contents, suggesting that the antigorite breakdown does not release large amounts of carbon (Alt *et al.*, 2012a).

Low or zero carbonate contents in ultramafic rocks from high pressure terrains may record either low initial carbon contents, or removal of carbon during metamorphism. Most

serpentinites have lower carbonate contents than the bulk composition investigated here (Alt *et al.*, 2013), so low initial carbonate is the most likely explanation for low carbonate in metamorphosed ultramafic rocks.

If metamorphism in natural systems is represented well by the calculations presented here then a significant reduction in carbon content by devolatilisation can only be achieved by infiltration of external, out of equilibrium fluids (e.g. Gorman *et al.*, 2006). Infiltrating fluids would also need to contain less CO_2 than that required for equilbrium with the carbonate phases. However, predicted CO_2 solubilities are so low that significant quantities of external fluids would be required to decarbonate to any great extent. For example, if 5% of the carbon is lost by dissolution in the water produced locally, then focussing of pure water from a volume twenty times the size of the original volume is required to achieve complete carbonate dissolution. Consideration of lithologies other than ultramafic does not change this value significantly; the high water content of serpentine means that ultramafic rocks produce the same order of magnitude quantity of water during metamorphism as metasediments or metabasalts. The likelihood of infitration of such fluids in the required quantities is discussed below.

If infiltration does not drive volatilisation then CO_2 retained in subducted lithospheric mantle is cycled into the deep mantle, where it may play a role in the genesis of mantle-derived melts in a variety of tectonic settings (e.g. Dasgupta & Hirschmann, 2007a,b, 2010). This cycling is of interest not only for present day processes, but also in the context of long term evolution of the composition of the mantle, and feedback relationships with the evolution of surface conditions and ocean composition (e.g. Evans, 2012).

Sulphur

It is calculated that less than 1% of sulphur is lost during prograde subduction metamorphism to 800 °C (Fig. 5c). H_2S fluid concentrations are always less than 0.1 mole%. If this is the case then sulphur subducted in ultramafic rocks is likely to stay in those rocks to pressures higher than 5 GPa. It has been proposed that only a relatively small proportion of subducted sulphur is recycled at arcs; Evans (2012) estimates that less than 20% of sulphur subducted in sediments, altered ocean crust and serpentinised

lithospheric mantle is recycled, while Jego & Dasgupta (2013) estimate that 15 to 30% of sulphur is returned to surface reservoirs by arc processes. The results of this work support these conclusions with most subducted sulphur likely to be transported to depths greater than 150 km.

However, the model results must be treated with caution; the activity-composition model for H_2S bearing fluids is calibrated only up to 0.5 GPa (Evans, 2010) and data are lacking for any confirmation of the applicability of the model at the pressures described here. Jego & Dasgupta (2013) and Jego & Dasgupta (2014) describe substantial H_2S solubilities in aqueous fluids in equilibrium with MORB at high pressures, though these experiments were performed at far more reducing conditions, and at substantially higher temperatures (950–1050 °C) than those investigated here. S_3^- has also been proposed to comprise the main sulphur-bearing species at subduction zone pressures and temperatures (Pokrovski & Dubrovinsky, 2011) although insufficient thermodynamic data is available for this species to allow its inclusion in the modelling.

There is also some evidence in natural systems for sulphur loss during metamorphism. Alt *et al.* (2012a) record S contents at Cerro del Amirez of 910 ± 730 ppm and 650 ± 620 ppm in antigorite serpentinites and olivine - orthopyroxene - chlorite harzburgites respectively. The heterogeneous distribution of sulphur within these rocks means that the statistical significance of the reduction in S content is low, with a students T-test p value greater than 0.2. Interestingly, the monosulphide sulphur (i.e. pyrrhotite) shows an unambiguously significant decrease in concentration ($p = 0.006$), from 719 ± 644 ppm to 202 ± 245 ppm, consistent with breakdown of this phase, potentially to form pyrite, which is present in most samples. Replacement of pyrrhotite by pyrite with increasing temperature would be consistent with the model results (Fig. 1). Debret *et al.* (2014a) present results from four different Alpine localities with different geodynamic histories that may suggest a decrease in sulphur content with increasing metamorphic grade.

Under these circumstances, the results for sulphur must be treated as semi-quantitative and further experimental work is required to constrain the solubility of sulphur in metamorphic fluids at high pressures and temperatures.

Redox budget

The redox budget of the model open system increases by about 40% between 350 and 850°C. About a third of this increase is due to methane loss at the brucite-out reaction, and most of the other two thirds is associated with dehydration during antigorite breakdown 6e. These increases in redox budget are accommodated by changes in the mode of pyrite and magnetite. The increase in redox budget is accommodated by pyrite growth and, to a lesser extent, to the increasing increasing ferric iron content of silicate phases.

More methane is produced on the hot geotherm, so the geothermal regime under which lithospheric mantle is subducted may affect the redox budget evolution of subducted material. The model predicts that slab subducted on cold geotherms are likely to have a lower redox budget than that subducted on hot geotherms. This result is consistent with observations by Evans (2012) that the redox budget of arc products is higher for rapidly converging, cold geotherms, since negative redox budget would not transfer to the sub-arc mantle when methane is not produced. However, this study addresses only one of the lithologies that can contribute to the redox budget of the sub-arc mantle, and the redox budget transfer discussed here may not be a first order control on the redox budget of sub-arc mantle.

In the closed system, the electrons carried by the methane are redistributed into the rock as metamorphism proceeds (compare Figs 6e and 7e), and the magnetite mode drops by about 1/3 as a consequence. Thus the extent to which the system was open during metamorphism has a potentially significant effect on the subducted redox budget carried to depth, see discussion below.

Magnetite and pyrite hold most of the redox budget in the rocks modelled, so the modes of these phases have potential as a proxy for the redox budget of ultramafic rocks. Scambelluri *et al.* (2014) records common magnetite and chromite associated with pyrrhotite and pentlandite in chlorite harzburgites at Cima di Gagnone, but only sparse, small oxide grains (unidentified) and rare sulphides in garnet peridotites. At first sight, this change suggests that redox budget decreases with garnet formation. It is likely, however, that ferric iron is likely to enter garnet once it forms, but the modelling does not

include ferric iron in garnet (see methods), so changes in redox budget cannot be inferred at this locality without knowledge of the ferric iron content of the garnet.

Effect of water loss on arc magmatism

A wide range of explanations have been proposed to explain the relationship between the location of volcanic arcs and subduction-related processes (e.g. Schmidt & Poli, 1998; Grove *et al.*, 2012). These explanations usually involve metamorphic and melting reactions that are proposed to occur either in the slab or in the sub-arc mantle (England & Katz, 2010). Expected depths of fluid release for the brucite to olivine and antigorite to orthpyroxene, olivine and chlorite reactions were plotted in conjunction with the England & Katz (2010) dataset of depths from arc to slab versus the product of subduction rate and slab dip (Fig. 9a). The England & Katz (2010) dataset has a negative slope on this figure, while the slope of depths at which fluid is released as a function of slab velocity is positive, i.e. the trend of the volcanic arc - slab depth data is opposite to that expected if metamorphic devolatilisation of hydrated ultramafic rocks contributes to arc volcanism in a direct and simple way. Slow subduction, which has the hotter geotherm, produces fluids via devolatilisation of minerals in ultramafic lithologies at relatively shallow depths (45–75 km), but in fact these slabs do not produce arcs until the slab has reached much greater depths (around 120 km), where the fluid would be expected to be long gone. A similar argument, in reverse, applies for rapid subduction, which has the colder geotherm. Thus devolatilisation of ultramafic lithologies seems unlikely to have a direct relationship with the production of the volcanic arc, consistent with the proposals of England & Katz (2010).

Nevertheless, convincing evidence suggests that the signature of dehydrating serpentinite can be seen in volcanic rocks at arc fronts (e.g. Tonarini *et al.*, 2011; Pabst *et al.*, 2012; Scambelluri & Tonarini, 2012). For example, Walker *et al.* (2009) measured B and Li content in Quaternary arc rocks associated with subduction of the Cocos plate below southeastern Guatemala and western El Salvador. Enrichments of B, Cs and Cl in arc rocks were taken to record a pulse of fluids from dehydrating serpentinite at 85–100 km depth. This depth is approximately consistent with those calculated by the model presented here.

Effects of fluid loss on seismic activity

The pressure–temperature conditions for the brucite- and antigorite-breakdown reactions were plotted in conjunction with the the range of conditions inferred for earthquakes within subducting slabs by Abers *et al.* (2013) (Fig. 9b). The conditions of brucite breakdown lie within the envelope of inferred pressure–temperature conditions for earthquake sources, and the slope in pressure–temperature conditions space is similar for the devolatilisation and earthquake datasets for hot and cold slabs. It is therefore possible that a link between fluid release and seismic activity exists, as suggested by previous workers (e.g. Abers *et al.*, 2013). The match is better than for previous comparisons of peridotite dehydration with earthquake production that use older thermodynamic simulations (e.g. Abers *et al.*, 2013).

Characteristics of fluid flow

Convenient end-members used to describe fluid production in metamorphism rocks are the closed system 'balloon' model, in which all fluid is retained, which is physically implausible, and a completely open system, where all fluid is expelled as soon as it is generated by devolatilisation reactions. Calculated results for the ultramafic lithologies investigated here show a similar evolution for most parameters in closed and open systems with the notable exception of pyrite and magnetite modes, and redox budget, which are discussed in detail above. Given that most rocks in subduction zones are likely to have undergone open system metamorphism, the redox budget effects of fluid loss are likely to be significant, but are difficult to assess unless the initial redox budget of the rock is known.

Fluid that leaves its host rock and infiltrates other rocks can transfer elements such as C and S, and redox budget between lithologies, or into the sub-arc mantle. If fluid migrates into veins without much pervasive interaction with surrounding rocks then there may be limited, or no, subsequent recorded fluid:rock interaction. If, on the other hand, fluid flows pervasively through overlying rocks as it escapes, then that fluid may drive reactions as it infiltrates those rocks (e.g. Gorman *et al.*, 2006). The effectiveness with which fluids drive reaction in infiltrated lithologies is related to the extent to which the fluids are out of equilibrium with that lithology. Fluids passing down a gentle temperature and pressure

gradient within a lithology identical to the one in which they formed will drive little reaction and are likely to be hard to detect unless a distinct isotopic signature can be recognised. On the other hand, fluids that cross lithological boundaries and infiltrate lithologies very different to those from where they originated are likely to be substantially out of equilibrium with those lithologies and drive substantial amounts of reaction in order to attain equilibrium.

Modelling of lithium isotope data in mafic rocks adjacent to high pressure veins suggests that pulses of devolatilised fluids transfer through the slab in relatively narrow conduits on a timescale of a few hundred years (John *et al.*, 2012). This channelisation of fluid is consistent with the observations of Spandler *et al.* (2011). It therefore seems likely the pulse of methane-bearing fluid that is calculated to be produced on hot slab geotherms is removed from the immediate vicinity of its production by channelised flow, but its ultimate fate is unknown.

Fluids lost from ultramafic rocks that do not underlie sediments and/or ocean crust within the subducting slab may have a greater effect on their surrounding lithologies. Scambelluri *et al.* (2014) suggest that ultramafic rocks at Cima di Gagnone rocks interacted with a variety of other rock types and fluids in a highly complex and mobile slab interface. In this case, fluids would infiltrate rocks more easily than in a slab environment, and, just as importantly, fluids released by dehydrating ultramafic rocks could drive reaction in surrounding lithologies. Similarly, Shimizu *et al.* (2013) proposed that samples from Erro Tobbio underwent high pressure metamorphism in a sub-arc mantle environment. Here, the rocks could have been affected by slab-derived fluids, and, indeed, the trace element contents are consistent with interaction with sediment-derived fluids. Additionally, fluids lost from ultramafic lithologies in the sub-arc mantle environment may be less channelled than in the slab, and could therefore drive reaction in surrounding lithologies more efficiently. However, there is insufficient evidence, at present, to assess this idea in a robust way.

The effects of redox budget changes on sub-arc mantle and the deep mantle

Addition of redox budget lost from the subducting slab in the form of oxidised species in fluids has been proposed by a number of workers to explain the oxidised nature of some arc magmas (e.g. Kelley & Cottrell, 2009; Evans & Tomkins, 2011). However, the results of the models suggest that the fluids released carry only relatively reduced species such as methane and H_2S in fluids. The loss of such fluids causes an increase in the rock redox budget of about a third, which is associated with an increase in ΔFMQ of a few tenths of a log unit. Thus, if the calculations presented here provide an acceptable representation of real systems, then addition of oxidised species to sub-arc settings must be from metasediments or metabasalts, or in species other than those considered here.

Species not included in the model that can transfer redox budget are ferric iron in aqueous solution, sulphate or S_3^- in aqueous solution, or silicate-rich aqueous fluids. Existing experimental evidence suggests that the solubility of ferric iron in aqueous fluids is too low to make a significant contribution to ferric iron transfer at moderate pressures and in solutions with moderate salinities (Wykes *et al.*, 2008). This conclusion is consistent with observations of metaserpentinites that suggest iron is not mobile on length-scales of greater than a few cm (Frost *et al.*, 2013). With respect to sulphur, the limited experimental evidence available suggests that H_2S or S_3^-, rather than sulphate, is the stable sulphur-bearing fluid species at the likely oxygen fugacities during metamorphism (Reed & Palandri, 2006; Pokrovski & Dubrovinsky, 2011; Jego & Dasgupta, 2013; Jacquemet *et al.*, 2014). S_3^- could transfer redox budget, though much less than sulphate, so further study of the solubility and properties of this species are required. It has been proposed that silicate-rich aqueous fluids exist under the conditions associated with subduction (Ferrando *et al.*, 2005), and such fluids could carry ferric iron. However, recent experimental work has found no evidence of such fluids in equilibrium with ultramafic rocks at temperatures to 800°C and pressures to 4 GPa (Spandler *et al.*, 2014). Nevertheless, assemblages that include oxidised iron- and sulphur-bearing minerals, such as hematite and anhydrite, exist in veins in mafic high pressure rocks (Philippot & Selverstone, 1991; Liu *et al.*, 2001; Ferrando *et al.*, 2005), and Alt *et al.* (2012a) used sulphur isotopes to infer that the sulphur lost at Cerro del Almirez during antigorite breakdown formed sulphate species.

This evidence suggests that solute-rich fluids that can carry sulphate and ferric iron may exist in subduction zones, so the possibility that these fluids make a contribution to redox transport cannot be excluded.

Another significant result of this study is the calculated increase in ΔFMQ from ΔFMQ -1 at 350 °C to over ΔFMQ+3 at 850 °C at constant redox budget (Fig. 4). Thus lithospheric mantle that becomes mechanically mixed with asthenospheric mantle, at sub-arc depths or elsewhere, has a higher ΔFMQ than the material with which is mixing and will increase its average redox budget, though ΔFMQ may not change much if aO_2 is well buffered. To some extent this is an intuitive result given the relatively oxidised nature of hydrated lithosphere. Experimental studies often use buffers such as NiO/Ni or CoO/O to control a_{O_2} in order to mitigate the effects of hydrogen migration through their platinum capsules. Such studies may be limited in their capacity to reveal the evolution of redistribution of redox-sensitive phases unless changing ΔFMQ is taken into account.

If redox budget carried by subducted hydrated lithospheric mantle is indeed added to the deep mantle then the consequences, integrated over geological time, may be that of a slow increase in the oxidation state of the mantle. Preliminary calculations suggest that redox budget added to the mantle by subduction could make a measurable difference to mantle redox state on timescales of about 1 Ga (Evans, 2012). However, subducted lithospheric mantle is likely to have been less oxidised than it is today prior to the second great oxidation event (GOE) at 550 Ma. Thus, changes to mantle redox state as a result of subduction may not occur until hundreds of millions of years in the future.

ACKNOWLEDGMENTS

KE acknowledges support from ARC DP1094075 and ARC FT120100579. Rosalind Crossley is thanked for discussions about the Alpine thin sections. RP acknowledges support from ARC DP0987731. We thank T. Holland for re-assessing the experimental data for antigorite in `ds62`, G. Rebay for her preliminary thermodynamic model for antigorite, and J. Diener for preliminary `ds62`-savvy models for clinoamphibole and clinopyroxene. J. Alt, J. Padrón-Navarta and G. Yaxley are thanked for perceptive reviews that improved the manuscript. This is TiGeR publication number 588.

References

Abers, G. A., Nakajima, J., van Keken, P. E., Kita, S. & Hacker, B. R., 2013. Thermal-petrological controls on the location of earthquakes within subducting plates. *Earth and Planetary Science Letters*, **369**, 178–187.

Alt, J. C., Garrido, C. J., Shanks, W. C., Turchyn, A., Padrón-Navarta, J. A., Sanchez-Vizcaino, V. L., Pugnaire, M. T. G. & Marchesi, C., 2012a. Recycling of water, carbon, and sulfur during subduction of serpentinites: A stable isotope study of Cerro del Almirez, Spain. *Earth and Planetary Science Letters*, **327**, 50–60.

Alt, J. C., Schwarzenbach, E. M., Frueh-Green, G. L., Shanks, W. C., Bernasconi, S. M., Garrido, C. J., Crispini, L., Gaggero, L., Padrón-Navarta, J. A. & Marchesi, C., 2013. The role of serpentinites in cycling of carbon and sulfur: Seafloor serpentinization and subduction metamorphism. *Lithos*, **178**, 40–54.

Alt, J. C., Shanks, W. C., Crispini, L., Gaggero, L., Schwarzenbach, E. M., Fruh-Green, G. L. & Bernasconi, S. M., 2012b. Uptake of carbon and sulfur during seafloor serpentinization and the effects of subduction metamorphism in Ligurian peridotites. *Chemical Geology*, **322**, 268–277.

Banfield, J. F. & Bailey, S. W., 1996. Formation of regularly interstratified serpentine-chlorite minerals by tetrahedral inversion in long-period serpentine polytypes. *American Mineralogist*, **81**, 79–91.

Barnes, S. J., Wells, M. A. & Verrall, M. R., 2009. Effects of magmatic processes, serpentinization, and talc-carbonate alteration on sulfide mineralogy and ore textures in the Black Swan disseminated nickel sulfide deposit, Yilgarn craton. *Economic Geology*, **104**(4), 539–562.

Barnicoat, A. C. & Cartwright, I., 1995. Focused fluid-flow during subduction - oxygen-isotope data from high-pressure ophiolites of the Western Alps. *Earth and Planetary Science Letters*, **132**(1-4), 53–61.

Bazylev, B. A., Ledneva, G. V., Kononkova, N. N. & Ishiwatari, A., 2013. High-pressure

ultramafics in the lower crustal rocks of the Pekul'ney complex, central Chukchi Peninsula. 1. Petrography and mineralogy. *Petrology*, **21**(3), 221–248.

Berry, A. J., Yaxley, G. M., Woodland, A. B. & Foran, G. J., 2010. A XANES calibration for determining the oxidation state of iron in mantle garnet. *Chemical Geology*, **278**(1-2), 31–37.

Beslier, M. O., Royer, J. Y., Girardeau, J., Hill, P. J., Boeuf, E., Buchanan, C., Chatin, F., Jacovetti, G., Moreau, A., Munschy, M., Partouche, C., Robert, U. & Thomas, S., 2004. A wide ocean-continent transition along the south-west Australian margin: first results of the MARGAU/MD110 cruise. *Bulletin De La Societe Geologique De France*, **175**(6), 629–641.

Bromiley, G. D. & Pawley, A. R., 2003. The stability of antigorite in the systems MgO-SiO_2-H_2O (MSH) and MgO-Al_2O_3-SiO_2-H_2O (MASH): The effects of Al^{3+} substitution on high-pressure stability. *American Mineralogist*, **88**(1), 99–108.

Cannat, M., Fontaine, F. & Escartin, J., 2010. *Serpentinization and associated hydrogen and methane fluxes at slow spreading ridges*, volume 188 of *Geophysical monograph series*, 440 pp. American Geophysical Union, Washington, DC.

Cannat, M., Lagabrielle, Y., Bougault, H., Casey, J., deCoutures, N., Dmitriev, L. & Fouquet, Y., 1997. Ultramafic and gabbroic exposures at the Mid-Atlantic Ridge: geological mapping in the 15 degrees N region. *Tectonophysics*, **279**(1-4), 193–213. Times Cited: 109 Cannat, M Lagabrielle, Y Bougault, H Casey, J deCoutures, N Dmitriev, L Fouquet, Y.

Clarke, G. L., Powell, R. & Fitzherbert, J. A., 2006. The lawsonite paradox: a comparison of field evidence and mineral equilibria modelling. *Journal of Metamorphic Geology*, **24**(8), 715–725.

Cressey, G., Cressey, B. A. & Wicks, F. J., 2008. The significance of the aluminium content of a lizardite at the nanoscale: the role of clinochlore as an aluminium sink. *Mineralogical Magazine*, **72**(3), 817–825.

Dale, C. W., Burton, K. W., Pearson, D. G., Gannoun, A., Alard, O., Argles, T. W. & Parkinson, I. J., 2009. Highly siderophile element behaviour accompanying subduction of oceanic crust: Whole rock and mineral-scale insights from a high-pressure terrain. *Geochimica Et Cosmochimica Acta*, **73**(5), 1394–1416.

Dasgupta, R. & Hirschmann, M. M., 2007a. Effect of variable carbonate concentration on the solidus of mantle peridotite. *American Mineralogist*, **92**(2-3), 370–379.

Dasgupta, R. & Hirschmann, M. M., 2007b. A modified iterative sandwich method for determination of near-solidus partial melt compositions. II. Application to determination of near-solidus melt compositions of carbonated peridotite. *Contributions to Mineralogy and Petrology*, **154**(6), 647–661.

Dasgupta, R. & Hirschmann, M. M., 2010. The deep carbon cycle and melting in Earth's interior. *Earth and Planetary Science Letters*, **298**(1-2), 1–13.

Dasgupta, R., Hirschmann, M. M. & Dellas, N., 2005. The effect of bulk composition on the solidus of carbonated eclogite from partial melting experiments at 3 GPa. *Contributions to Mineralogy and Petrology*, **149**(3), 288–305. Times Cited: 49 Dasgupta, R Hirschmann, MM Dellas, N.

Dasgupta, R., Hirschmann, M. M. & Withers, A. C., 2004. Deep global cycling of carbon constrained by the solidus of anhydrous, carbonated eclogite under upper mantle conditions. *Earth and Planetary Science Letters*, **227**(1-2), 73–85. Times Cited: 138 Dasgupta, R Hirschmann, MM Withers, AC.

Dauphas, N., Craddock, P. R., Asimow, P. D., Bennett, V. C., Nutman, A. P. & Ohnenstetter, D., 2009. Iron isotopes may reveal the redox conditions of mantle melting from Archean to Present. *Earth and Planetary Science Letters*, **288**(1-2), 255–267.

Debret, B., Andreani, M., Munoz, M., Bolfan-Casanova, N., Carlut, J., Nicollet, C., Schwartz, S. & Trcera, N., 2014a. Evolution of Fe redox state in serpentine during subduction. *Earth and Planetary Science Letters*, **400**, 206–218.

Debret, B., Koga, K. T., Nicollet, C., Andreani, M. & Schwartz, S., 2014b. F, Cl and S

input via serpentinite in subduction zones: implications for the nature of the fluid released at depth. *Terra Nova*, **26**(2), 96–101.

Dijkstra, A. H., Sergeev, D. S., Spandler, C., Pettke, T., Meisel, T. & Cawood, P. A., 2010. Highly Refractory Peridotites on Macquarie Island and the Case for Anciently Depleted Domains in the Earth's Mantle. *Journal of Petrology*, **51**(1-2), 469–493. Times Cited: 12 Dijkstra, Arjan H. Sergeev, Dmitry S. Spandler, Carl Pettke, Thomas Meisel, Thomas Cawood, Peter A. 5th Lherzolite Conference Sep, 2008 Shasta City, CA.

England, P. C. & Katz, R. F., 2010. Melting above the anhydrous solidus controls the location of volcanic arcs. *Nature*, **467**(7316), 700–U84.

Evans, B. W., 2004. The serpentinite multisystem revisited: Chrysotile is metastable. *International Geology Review*, **46**(6), 479–506.

Evans, B. W., 2008. Control of the products of serpentinization by the Fe(2)Mg(1) exchange potential of olivine and orthopyroxene. *Journal of Petrology*, **49**(10), 1873–1887.

Evans, B. W., Dyar, M. D. & Kuehner, S. M., 2012. Implications of ferrous and ferric iron in antigorite. *American Mineralogist*, **97**(1), 184–196.

Evans, K., 2010. A test of the viability of fluid-wall rock interaction mechanisms for changes in opaque phase assemblage in metasedimentary rocks in the Kambalda-St. Ives goldfield, Western Australia. *Mineralium Deposita*, **45**(2), 207–213.

Evans, K. & Powell, R., 2006. A method for activity calculations in saline and mixed solvent solutions at elevated temperature and pressure: A framework for geological phase equilibria calculations. *Geochimica et Cosmochimica Acta*, **70**(22), 5488–5506.

Evans, K., Powell, R. & Holland, T., 2010. Internally consistent data for sulphur-bearing phases and application to the construction of pseudosections for mafic greenschist facies rocks in Na_2O-CaO-K_2O-FeO-MgO-Al_2O_3-SiO_2-CO_2-O-S-H_2O. *Journal of Metamorphic Geology*, **28**, 667–687.

Evans, K. & Tomkins, A., 2011. The relationship between subduction zone redox budget and arc magma fertility. *Earth and Planetary Science Letters*, **308**, 401–409.

Evans, K., Tomkins, A., Cliff, J. & Fiorentini, M. L., 2014. Insights into subduction zone sulfur recycling from isotopic analysis of eclogite-hosted sulfides. *Chemical Geology*, **365**, 1–19.

Evans, K. A., 2006. Redox decoupling and redox budgets: Conceptual tools for the study of earth systems. *Geology*, **34**(6), 489–492.

Evans, K. A., 2012. The redox budget of subduction zones. *Earth Science Reviews*, **113**, 11–32.

Evans, K. A., Powell, R. & Frost, B. R., 2013. Using equilibrium thermodynamics in the study of metasomatic alteration, illustrated by an application to serpentinites. *Lithos*, **168**, 67–84.

Ferrando, S., Frezzotti, M. L., Dallai, L. & Compagnoni, R., 2005. Multiphase solid inclusions in UHP rocks (Su-Lu, China): Remnants of supercritical silicate-rich aqueous fluids released during continental subduction. *Chemical Geology*, **223**(1-3), 68–81.

Ferry, J. M., 1981. Petrology of graphitic sulfide-rich schists from South-Central Maine - an example of desulfidation during prograde regional metamorphism. *American Mineralogist*, **66**(9-10), 908–931.

Fitzherbert, J. A., Clarke, G. L., Marmo, B. & Powell, R., 2004. The origin and P-T evolution of peridotites and serpentinites of NE New Caledonia: prograde interaction between continental margin and the mantle wedge. *Journal of Metamorphic Geology*, **22**(4), 327–344.

Frost, B. R., 1985. On the stability of sulfides, oxides, and native metals in serpentinite. *Journal of Petrology*, **26**(1), 31–63.

Frost, B. R., Evans, K. A., Swapp, S. M., Beard, J. S. & Mothersole, F. E., 2013. The process of serpentinization in dunite from New Caledonia. *Lithos*, **178**, 24–39.

Fry, N. & Barnicoat, A. C., 1987. The tectonic implications of high-pressure metamorphism in the Western Alps. *Journal of the Geological Society*, **144**, 653–659.

Giacometti, F., Evans, K., Rebay, G., Cliff, J., Tomkins, A., Rossetti, P., Vaggelli, G. & Adams, D., 2014. Sulfur isotope evolution in sulfide ores from Western Alps: Assessing the influence of subduction-related metamorphism. *Geochemistry Geophysics Geosystems*, **15**(10), 3808–3829.

Gole, M. J., Barnes, S. J. & Hill, R. E. T., 1987. The role of fluids in the metamorphism of komatiites, Agnew nickel deposit, Western Australia. *Contributions to Mineralogy and Petrology*, **96**(2), 151–162.

Gorman, P. J., Kerrick, D. M. & Connolly, J. A. D., 2006. Modeling open system metamorphic decarbonation of subducting slabs. *Geochemistry Geophysics Geosystems*, **7**.

Grove, T. L., Till, C. B. & Krawczynski, M. J., 2012. The role of H_2O in subduction zone magmatism. *Annual Review of Earth and Planetary Sciences*, **40**, 413–439.

Guiraud, M., Powell, R. & Rebay, G., 2001. H_2O in metamorphism and unexpected behaviour in the preservation of metamorphic assemblages. *Journal of Metamorphic Geology*, **19**, 445–454.

Hirauchi, K., Katayama, I., Uehara, S., Miyahara, M. & Takai, Y., 2010. Inhibition of subduction thrust earthquakes by low-temperature plastic flow in serpentine. *Earth and Planetary Science Letters*, **295**(3-4), 349–357.

Holland, T. & Powell, R., 1996. Thermodynamics of order-disorder in minerals .2. Symmetric formalism applied to solid solutions. *American Mineralogist*, **81**(11-12), 1425–1437. NOV-DEC AMER MINERAL Alternate Journal: Am. Miner.

Holland, T. J. B. & Powell, R., 1998. An internally consistent thermodynamic data set for phases of petrological interest. *Journal of Metamorphic Geology*, **16**(3), 309–343.

Holland, T. J. B. & Powell, R., 2011. An improved and extended internally consistent thermodynamic dataset for phases of petrological interest, involving a new equation of state for solids. *Journal of Metamorphic Geology*, **29**(3), 333–383.

Jacquemet, N., Guillaume, D., Zwick, A. & Pokrovski, G. S., 2014. In situ Raman spectroscopy identification of the S-3(-) ion in S-rich hydrothermal fluids from synthetic fluid inclusions. *American Mineralogist*, **99**(5-6), 1109–1118.

Jego, S. & Dasgupta, R., 2013. Fluid-present melting of sulfide-bearing ocean-crust: Experimental constraints on the transport of sulfur from subducting slab to mantle wedge. *Geochimica Et Cosmochimica Acta*, **110**, 106–134.

Jego, S. & Dasgupta, R., 2014. The Fate of Sulfur During Fluid-Present Melting of Subducting Basaltic Crust at Variable Oxygen Fugacity. *Journal of Petrology*, **55**(6), 1019–1050. Times Cited: 0 Jego, Sebastien Dasgupta, Rajdeep.

John, T., Gussone, N., Podladchikov, Y. Y., Bebout, G. E., Dohmen, R., Halama, R., Klemd, R., Magna, T. & Seitz, H. M., 2012. Volcanic arcs fed by rapid pulsed fluid flow through subducting slabs. *Nature Geoscience*, **5**(7), 489–492.

Katayama, I., Hirauchi, H., Michibayashi, K. & Ando, J., 2009. Trench-parallel anisotropy produced by serpentine deformation in the hydrated mantle wedge. *Nature*, **461**(7267), 1114–U209.

Kelley, K. A. & Cottrell, E., 2009. Water and the oxidation state of subduction zone magmas. *Science*, **325**(5940), 605–607.

Kerrick, D. M. & Connolly, J. A. D., 1998. Subduction of ophicarbonates and recycling of CO_2 and H_2O. *Geology*, **26**(4), 375–378.

Lee, C. T. A., Leeman, W. P., Canil, D. & Li, Z. X. A., 2005. Similar V/Sc systematics in MORB and arc basalts: Implications for the oxygen fugacities of their mantle source regions. *Journal of Petrology*, **46**(11), 2313–2336.

Lee, C. T. A., Luffi, P., Chin, E. J., Bouchet, R., Dasgupta, R., Morton, D. M., Le Roux, V., Yin, Q. Z. & Jin, D., 2012. Copper systematics in arc magmas and implications for crust-mantle differentiation. *Science*, **336**(6077), 64–68.

Li, X. P., Rahn, M. & Bucher, K., 2004. Serpentinites of the Zermatt-Saas ophiolite complex and their texture evolution. *Journal of Metamorphic Geology*, **22**(3), 159–177.

Liu, J. B., Ye, K., Maruyama, S. N., Cong, B. L. & Fan, H. R., 2001. Mineral inclusions in zircon from gneisses in the ultrahigh-pressure zone of the Dabie Mountains, China. *Journal of Geology*, **109**(4), 523–535.

Mallmann, G. & O'Neill, H. S. C., 2009. The crystal/melt partitioning of V during mantle melting as a function of oxygen fugacity compared with some other elements (Al, P, Ca, Sc, Ti, Cr, Fe, Ga, Y, Zr and Nb). *Journal of Petrology*, **50**(9), 1765–1794.

Mevel, C., 2003. Serpentinization of abyssal peridotites at mid-ocean ridges. *Comptes Rendus Geoscience*, **335**(10-11), 825–852.

Mungall, J. E., 2002. Roasting the mantle: Slab melting and the genesis of major Au and Au-rich Cu deposits. *Geology*, **30**(10), 915–918.

Neumayr, P., Walshe, J., Hagemann, S., Petersen, K., Roache, A., Frikken, P., Horn, L. & Halley, S., 2008. Oxidized and reduced mineral assemblages in greenstone belt rocks of the St. Ives gold camp, Western Australia: vectors to high-grade ore bodies in Archaean gold deposits? *Mineralium Deposita*, **43**(3), 363–371.

Pabst, S., Zack, T., Savoy, I. P., Ludwig, T., Rost, D., Tonarini, S. & Vicenzi, E. P., 2012. The fate of subducted oceanic slabs in the shallow mantle: Insights from boron isotopes and light element composition of metasomatized blueschists from the Mariana forearc. *Lithos*, **132**, 162–179.

Padrón-Navarta, J. A., Hermann, J., Garrido, C. J., Sanchez-Vizcaino, V. L. & Gomez-Pugnaire, M. T., 2010. An experimental investigation of antigorite dehydration in natural silica-enriched serpentinite. *Contributions to Mineralogy and Petrology*, **159**(1), 25–42.

Padrón-Navarta, J. A., Sanchez-Vizcaino, V. L., Garrido, C. J. & Gomez-Pugnaire, M. T., 2011. Metamorphic record of high-pressure dehydration of antigorite serpentinite to chlorite harzburgite in a subduction setting (Cerro del Almirez, Nevado-Filabride Complex, Southern Spain). *Journal of Petrology*, **52**(10), 2047–2078.

Padrón-Navarta, J. A., Sanchez-Vizcaino, V. L., Hermann, J., Connolly, J. A. D., Garrido, C. J., Gomez-Pugnaire, M. T. & Marchesi, C., 2013. Tschermak's substitution in

antigorite and consequences for phase relations and water liberation in high-grade serpentinites. *Lithos*, **178**, 186–196.

Parkinson, I. J. & Arculus, R. J., 1999. The redox state of subduction zones: insights from arc-peridotites. *Chemical Geology*, **160**(4), 409–423.

Philippot, P. & Selverstone, J., 1991. Trace-element-rich brines in eclogitic veins - implications for fluid composition and transport during subduction. *Contributions to Mineralogy and Petrology*, **106**(4), 417–430.

Pitzer, K. S. & Sterner, S. M., 1994. Equations of state valid continuously from zero to extreme pressures for H_2O and CO_2. *Journal of Chemical Physics*, **101**(4), 3111–3116.

Pokrovski, G. S. & Dubrovinsky, L. S., 2011. The S-3(-) ion Is stable in geological fluids at elevated temperatures and pressures. *Science*, **331**(6020), 1052–1054.

Powell, R. & Holland, T. J. B., 1988. An internally consistent thermodynamic dataset with uncerainties and correlations: 3. Applications to geobarometry, worked examples and a computer program. *J. Met. Geol.*, **6**, 173–204.

Powell, R., White, R. W., Green, E. C. R., Holland, T. J. B. & Diener, J. F. A., 2014. On parameterizing thermodynamic descriptions of minerals for petrological calculations. *Journal of Metamorphic Geology*, **32**(3), 245–260.

Ranero, C. R. & Sallares, V., 2004. Geophysical evidence for hydration of the crust and mantle of the Nazca plate during bending at the north Chile trench. *Geology*, **32**(7), 549–552.

Rebay, G., Spalla, M. I. & Zanoni, D., 2012. Interaction of deformation and metamorphism during subduction and exhumation of hydrated oceanic mantle: Insights from the Western Alps. *Journal of Metamorphic Geology*, **30**(7), 687–702.

Reed, M. H. & Palandri, J., 2006. Sulfide mineral precipitation from hydrothermal fluids. *Sulfide Mineralolgy and Geochemistry*, **61**, 609–631.

Reinecke, T., 1991. Very-high-pressure metamorphism and uplift of coesite-bearing metasediments from the Zermatt-Saas Zone, Western Alps. *European Journal of Mineralogy*, **3**(1), 7–17.

Reinecke, T., 1998. Prograde high- to ultrahigh-pressure metamorphism and exhumation of oceanic sediments at Lago di Cignana, Zermatt-Saas Zone, western Alps. *Lithos*, **42**(3-4), 147–189.

Rosenberg, P., 1967. Subsolidus relations in the system $CaCO_3$-$MgCO_3$-$FeCO_3$ between 350° and 550°C. *The American Mineralogist*, **52**, 787–796.

Rüpke, L. H., Morgan, J. P., Hort, M. & Connolly, J. A. D., 2004. Serpentine and the subduction zone water cycle. *Earth and Planetary Science Letters*, **223**(1-2), 17–34.

Sánchez-Vizcaíno, V. L., Trommsdorff, V., Gomez-Pugnaire, M. T., Garrido, C. J., Muntener, O. & Connolly, J. A. D., 2005. Petrology of titanian clinohumite and olivine at the high-pressure breakdown of antigorite serpentinite to chlorite harzburgite (Almirez Massif, S. Spain). *Contributions to Mineralogy and Petrology*, **149**(6), 627–646.

Scambelluri, M., Pettke, T., Rampone, E., Godard, M. & Reusser, E., 2014. Petrology and Trace Element Budgets of High-pressure Peridotites Indicate Subduction Dehydration of Serpentinized Mantle (Cima di Gagnone, Central Alps, Switzerland). *Journal of Petrology*, **55**(3), 459–498.

Scambelluri, M. & Tonarini, S., 2012. Boron isotope evidence for shallow fluid transfer across subduction zones by serpentinized mantle. *Geology*, **40**(10), 907–910.

Schmidt, M. W. & Poli, S., 1998. Experimentally based water budgets for dehydrating slabs and consequences for arc magma generation. *Earth and Planetary Science Letters*, **163**(1-4), 361–379.

Schwartz, S., Guillot, S., Reynard, B., Lafay, R., Debret, B., Nicollet, C., Lanari, P. & Auzende, A. L., 2013. Pressure-temperature estimates of the lizardite/antigorite transition in high pressure serpentinites. *Lithos*, **178**, 197–210.

Shimizu, N., Scambelluri, M., Santiago Ramos, D. & Tonarini, S., 2013. Boron and sulfur isotopic variations during subduction of hydrated lithosphere: The Erro Tobbio case. *Mineralogical Magazine*, **77**, 2201.

Sillitoe, R. H., 2010. Porphyry copper systems. *Economic Geology*, **105**(1), 3–41.

Spandler, C., Hartmann, J., Faure, K., Mavrogenes, J. A. & Arculus, R. J., 2008. The importance of talc and chlorite "hybrid" rocks for volatile recycling through subduction zones; evidence from the high-pressure subduction melange of New Caledonia. *Contributions to Mineralogy and Petrology*, **155**(2), 181–198.

Spandler, C., Pettke, T. & Hermann, J., 2014. Experimental study of trace element release during ultrahigh-pressure serpentinite dehydration. *Earth and Planetary Science Letters*, **391**, 296–306.

Spandler, C., Pettke, T. & Rubatto, D., 2011. Internal and external fluid sources for eclogite-facies veins in the Monviso meta-ophiolite, Western Alps: implications for fluid flow in subduction zones. *Journal of Petrology*, **52**(6), 1207–1236.

Tonarini, S., Leeman, W. P. & Leat, P. T., 2011. Subduction erosion of forearc mantle wedge implicated in the genesis of the South Sandwich Island (SSI) arc: Evidence from boron isotope systematics. *Earth and Planetary Science Letters*, **301**(1-2), 275–284.

Toulmin, I., P. & Barton, J., P.Bl, 1964. Thermodynamic study of pyrite and pyrrhotite. *Geochimica et Cosmochimica Acta*, **28**, 641–671.

Ulmer, P. & Trommsdorff, V., 1995. Serpentine stability to mantle depths and subduction-related magmatism. *Science*, **268**(5212), 858–861.

van Keken, P. E., Kiefer, B. & Peacock, S. M., 2002. High-resolution models of subduction zones: Implications for mineral dehydration reactions and the transport of water into the deep mantle. *Geochemistry Geophysics Geosystems*, **3**.

Walker, J. A., Teipel, A. P., Ryan, J. G. & Syracuse, E., 2009. Light elements and Li isotopes across the northern portion of the Central American subduction zone. *Geochemistry Geophysics Geosystems*, **10**.

White, R. W., Powell, R. & Clarke, G. L., 2003. Prograde metamorphic assemblage evolution during partial melting of metasedimentary rocks at low pressures: Migmatites from Mt Stafford, central Australia. *Journal of Petrology*, **44**(11), 1937–1960.

White, R. W., Powell, R., Holland, T. J. B., Johnson, T. E. & Green, E. C. R., 2014. New mineral activity-composition relations for thermodynamic calculations in metapelitic systems. *Journal of Metamorphic Geology*, **32**(3), 261–286.

Wunder, B. & Schreyer, W., 1997. Antigorite: High pressure stability in the system MgO-SiO_2-H_2O (MSH). *Lithos*, **41**(1-3), 213–227.

Wykes, J. L., Newton, R. C. & Manning, C. E., 2008. Solubility of andradite, $Ca_3Fe_2Si_3O_{12}$, in a 10 mol% NaCl solution at 800 degrees C and 10 kbar: Implications for the metasomatic origin of grandite garnet in calc-silicate granulites. *American Mineralogist*, **93**(5-6), 886–892.

Yang, J. J. & Powell, R., 2006. Calculated phase relations in the system Na_2O-CaO-K_2O-FeO-MgO-Al_2O_3-SiO_2-H_2O with applications to UHP eclogites and whiteschists. *Journal of Petrology*, **47**(10), 2047–2071.

Yaxley, G. M. & Brey, G. P., 2004. Phase relations of carbonate-bearing eclogite assemblages from 2.5 to 5.5 GPa: implications for petrogenesis of carbonatites. *Contributions to Mineralogy and Petrology*, **146**(5), 606–619.

FIGURE CAPTIONS

Figure 1: Pressure-temperature pseudosection in the system CaFMASCOSH for a depleted ultramafic bulk composition. Magnesian carbonate, magnetite and H_2O-CO_2-CH_4-H_2S fluid in excess. Calculated with THERMOCALC v3.40i and `ds62`.

Figure 2: Mineral modes and fluid compositions for a depleted ultramafic bulk composition undergoing closed system metamorphism on the hot geotherm. Magnesian carbonate, magnetite and H_2O-CO_2-CH_4-H_2S fluid in excess. Calculated with THERMOCALC v3.40i and `ds62`.

Figure 3: Mineral modes and fluid compositions for a depleted ultramafic bulk composition undergoing closed system metamorphism on the cold geotherm. Magnesian carbonate, magnetite and H_2O-CO_2-CH_4-H_2S fluid in excess. Calculated with THERMOCALC v3.40i and `ds62`.

Figure 4: T-X_O isobaric section at 2.6 GPa showing mineral assemblages for a depleted ultramafic bulk composition in the system CaFMASCOSH for a depleted ultramafic bulk composition. Magnesian carbonate, magnetite and H_2O-CO_2-CH_4-H_2S fluid in excess. Calculated with THERMOCALC v3.40i and `ds62`. White lines are contours of ΔFMQ, i.e. $\log_{10} fO_2 - \log_{10} fO_{2,FMQ}$ where FMQ is the fayalite-magnetite-quartz buffer.

Figure 5: Contents of volatile components of a depleted ultramafic bulk composition undergoing open system metamorphism at 2.4 GPa. Magnesian carbonate, magnetite and H_2O-CO_2-CH_4-H_2S fluid in excess. Calculated with THERMOCALC v3.40i and `ds62`.

Figure 6: Mineral modes and compositional variables for a depleted ultramafic bulk composition undergoing open system metamorphism at 2.4 GPa. Magnesian carbonate, magnetite and H_2O-CO_2-CH_4-H_2S fluid in excess. Calculated with THERMOCALC v3.40i and `ds62`.

Figure 7: Mineral modes and compositional variables of a depleted ultramafic bulk composition undergoing closed system metamorphism at 2.4 GPa. Magnesian

carbonate, magnetite and H_2O-CO_2-CH_4-H_2S fluid in excess. Calculated with THERMOCALC v3.40i and `ds62`.

Figure 8: Textural relationships exhibited by ultramafic rocks metamorphosed at high pressures. a: Co-existing chlorite and antigorite in sample PF-001 (Pfulwe, Zermat-Saas, Western Alps, transmitted light, crossed polars; b: Pyrite in sample PF0-001, back scattered electron image; c: Chalcopyrite in sample PF-001, back scattered electron image; d: Talc rimmed by magnetite in sample PF-001 (transmitted light, crossed polars); e: Magnetite intergrown with late chlorite in sample LC-015 (transmitted light, crossed polars); f: Concentricallly zoned magnetite hosted by large carbonate porphyroblast in NC07-56 (reflected light, plane polarised); g: Complex multistage distribution of Ti-rich and Ti-poor magnetite with hematite in NC07-50 (reflected light, plane polarised); h: Carbonate-chlorite-magnetite veins in sample NC07-58 (transmitted light, crossed polars).

Figure 9. a: Comparison of expected depths of fluid release for the brucite to olivine and antigorite to orthpyroxene and chlorite reactions with the England & Katz (2010) dataset of depths from arc to slab. The x axis is the product of subduction rate and slab dip; b: Comparison of the pressure–temperature conditions for the brucite- and antigorite-breakdown with the the range of conditions inferred for earthquakes within subducting slabs by Abers *et al.* (2013).

TABLES

Table 1: Bulk composition used for figures

Oxide	Mole percent
SiO_2	25.72
Al_2O_3	0.14
FeO	2.85
MgO	38.98
CaO	0.14
H_2O	30.51
CO_2	1.72
O	-0.14
SO_2	0.09

1 FIGURES

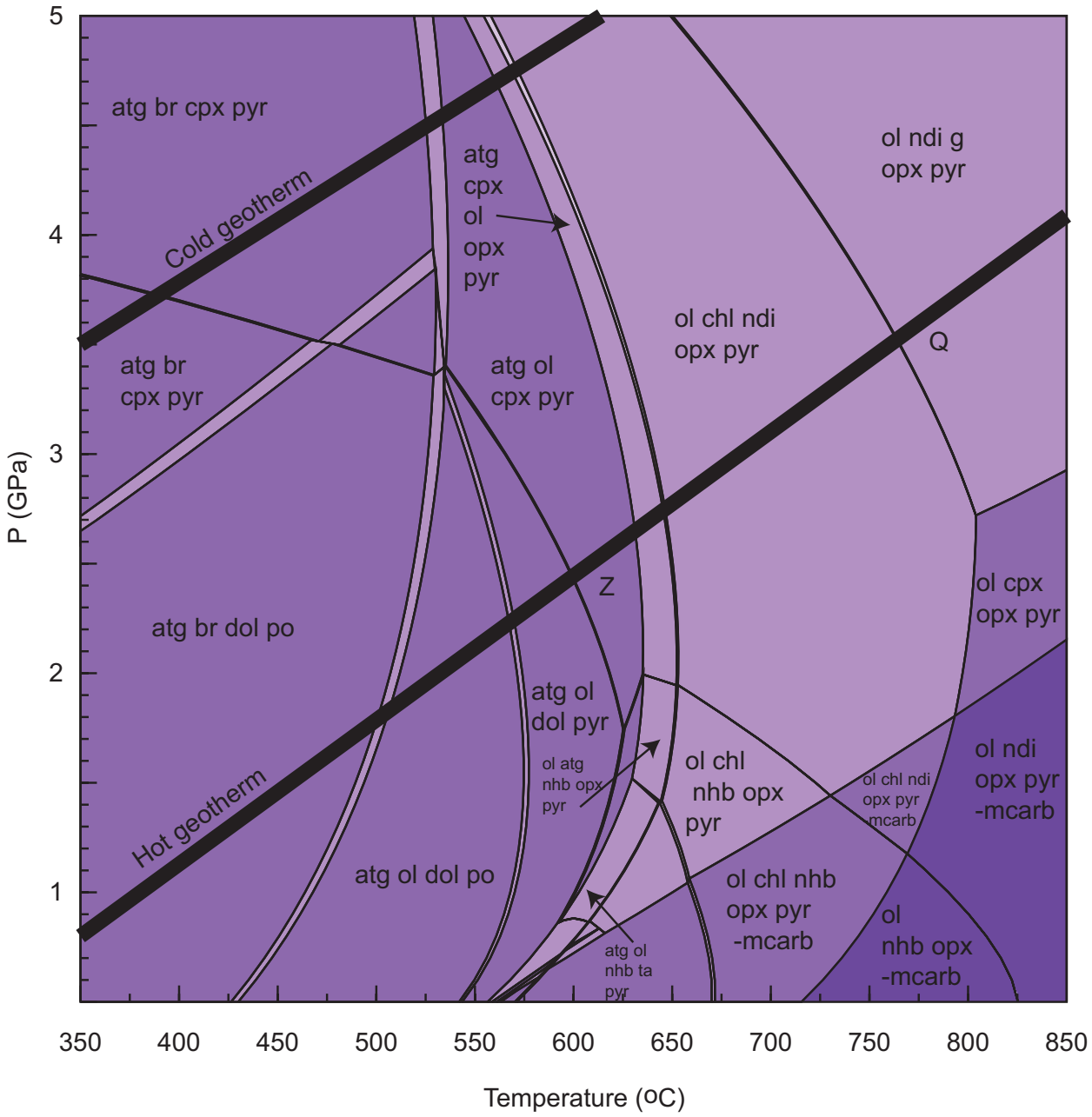

Figure 1:

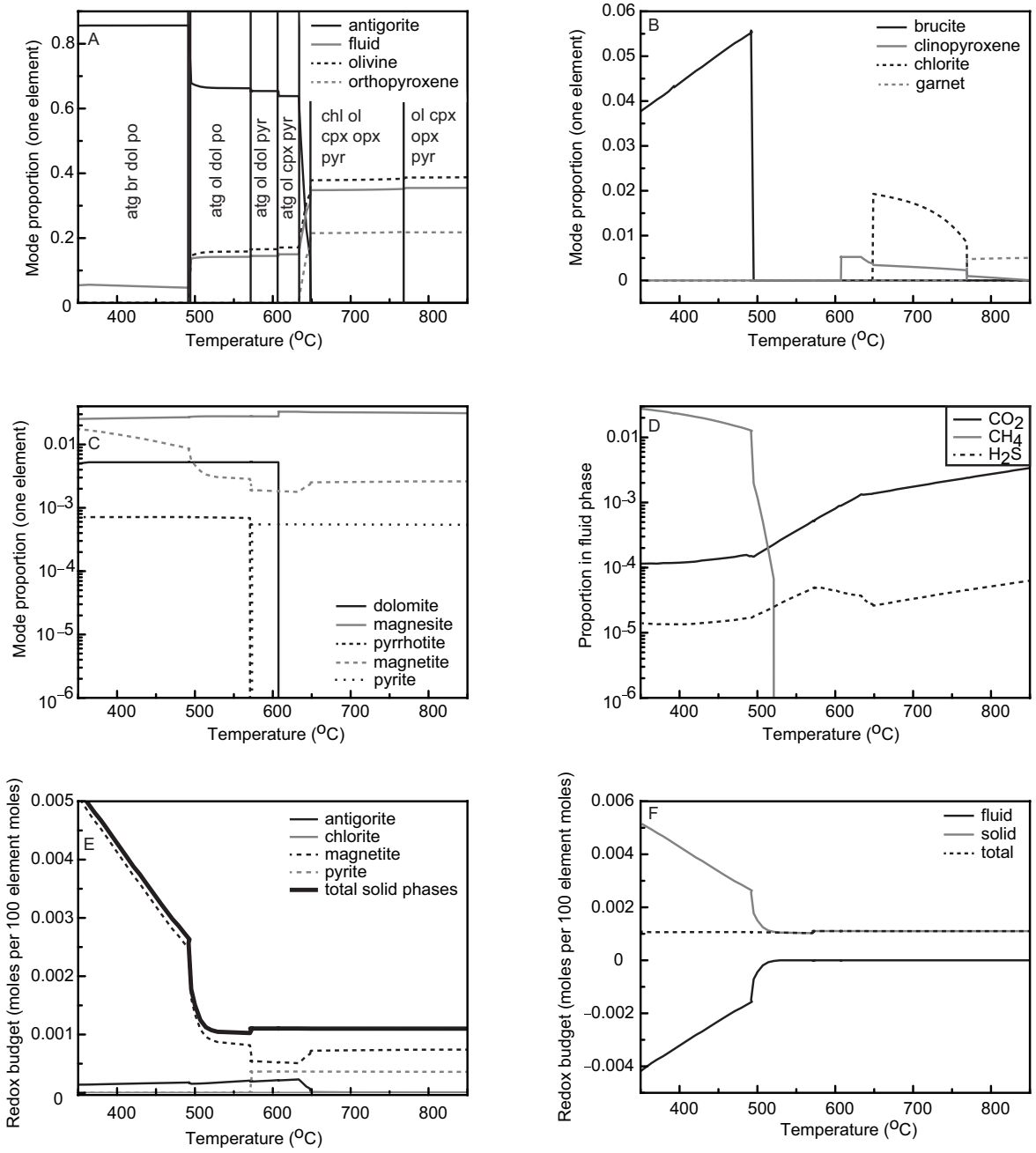
A
Mode proportion (one element)
Temperature (°C)
antigorite
fluid
olivine
orthopyroxene
atg br dol po
atg ol dol po
atg ol dol pyr
atg ol cpx pyr
chl ol cpx opx pyr
ol cpx opx pyr
B
brucite
clinopyroxene
chlorite
garnet
C
dolomite
magnesite
pyrrhotite
magnetite
pyrite
D
Proportion in fluid phase
CO2
CH4
H2S
E
Redox budget (moles per 100 element moles)
antigorite
chlorite
magnetite
pyrite
total solid phases
F
fluid
solid
total

Figure 2:

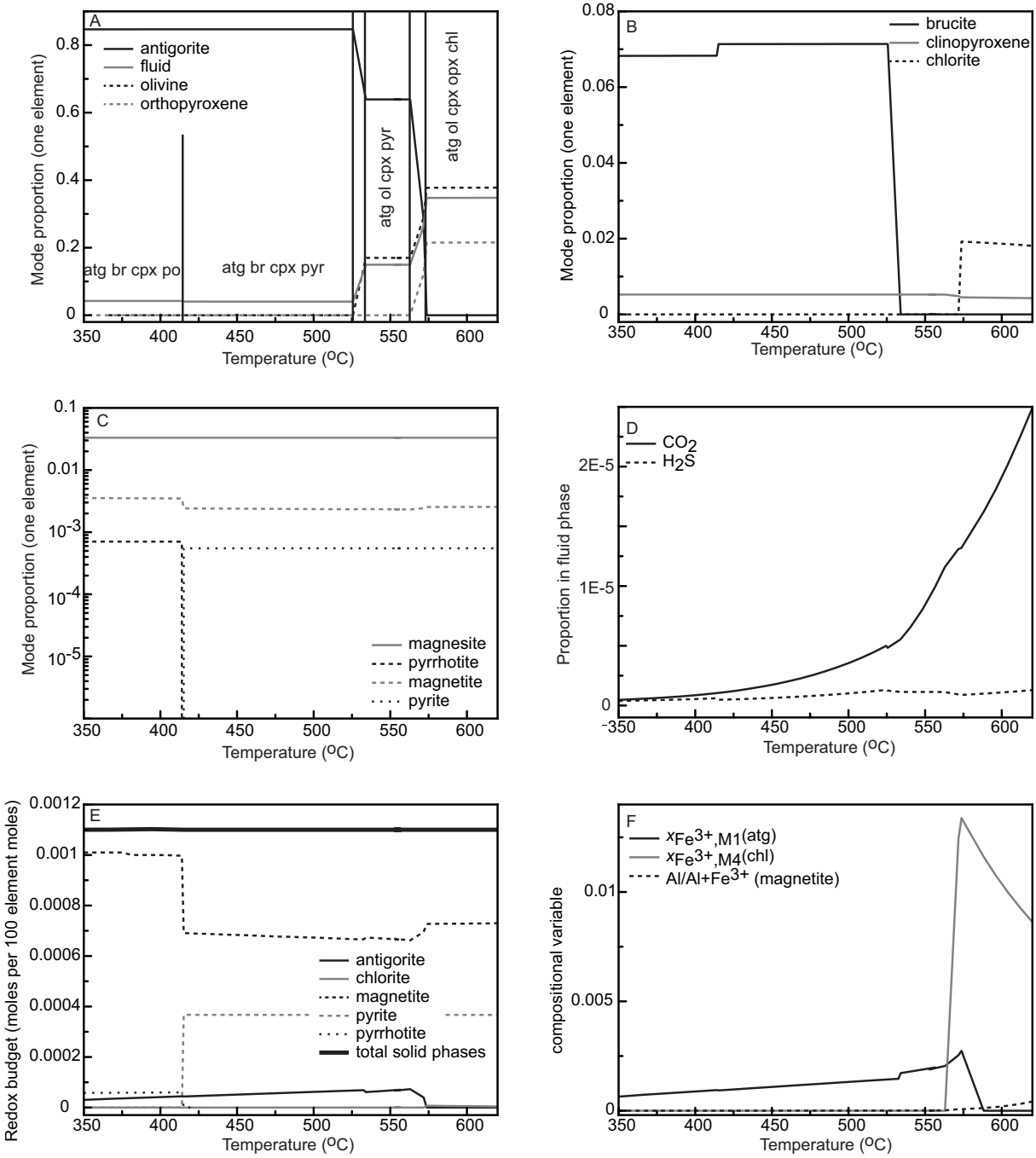
A
antigorite
fluid
olivine
orthopyroxene
atg br cpx po
atg br cpx pyr
atg ol cpx pyr
atg ol cpx opx chl
Mode proportion (one element)
Temperature (°C)
B
brucite
clinopyroxene
chlorite
C
magnesite
pyrrhotite
magnetite
pyrite
D
CO2
H2S
Proportion in fluid phase
E
antigorite
chlorite
magnetite
pyrite
pyrrhotite
total solid phases
Redox budget (moles per 100 element moles)
F
xFe3+,M1(atg)
xFe3+,M4(chl)
Al/Al+Fe3+ (magnetite)
compositional variable

Figure 3:

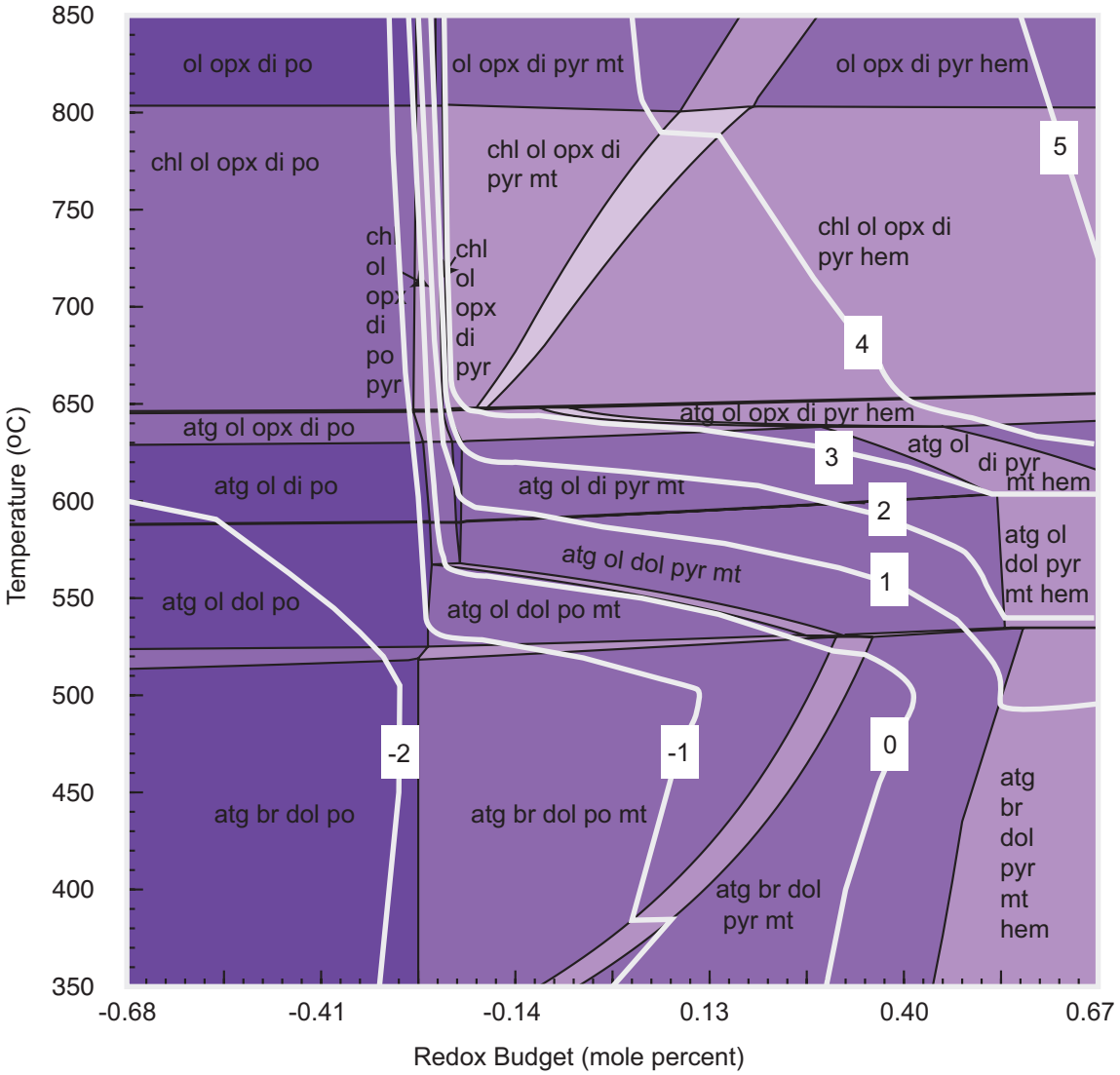
ol opx di po
ol opx di pyr mt
ol opx di pyr hem
chl ol opx di po
chl ol opx di pyr mt
chl ol opx di pyr hem
5
4
atg ol opx di po
atg ol opx di pyr hem
atg ol di po
atg ol di pyr mt
3
2
atg ol dol pyr mt
1
atg ol dol po
atg ol dol po mt
-2
-1
0
atg br dol po
atg br dol po mt
atg br dol pyr mt
atg br dol pyr mt hem
Temperature (oC)
Redox Budget (mole percent)
850
800
750
700
650
600
550
500
450
400
350
-0.68
-0.41
-0.14
0.13
0.40
0.67

Figure 4:

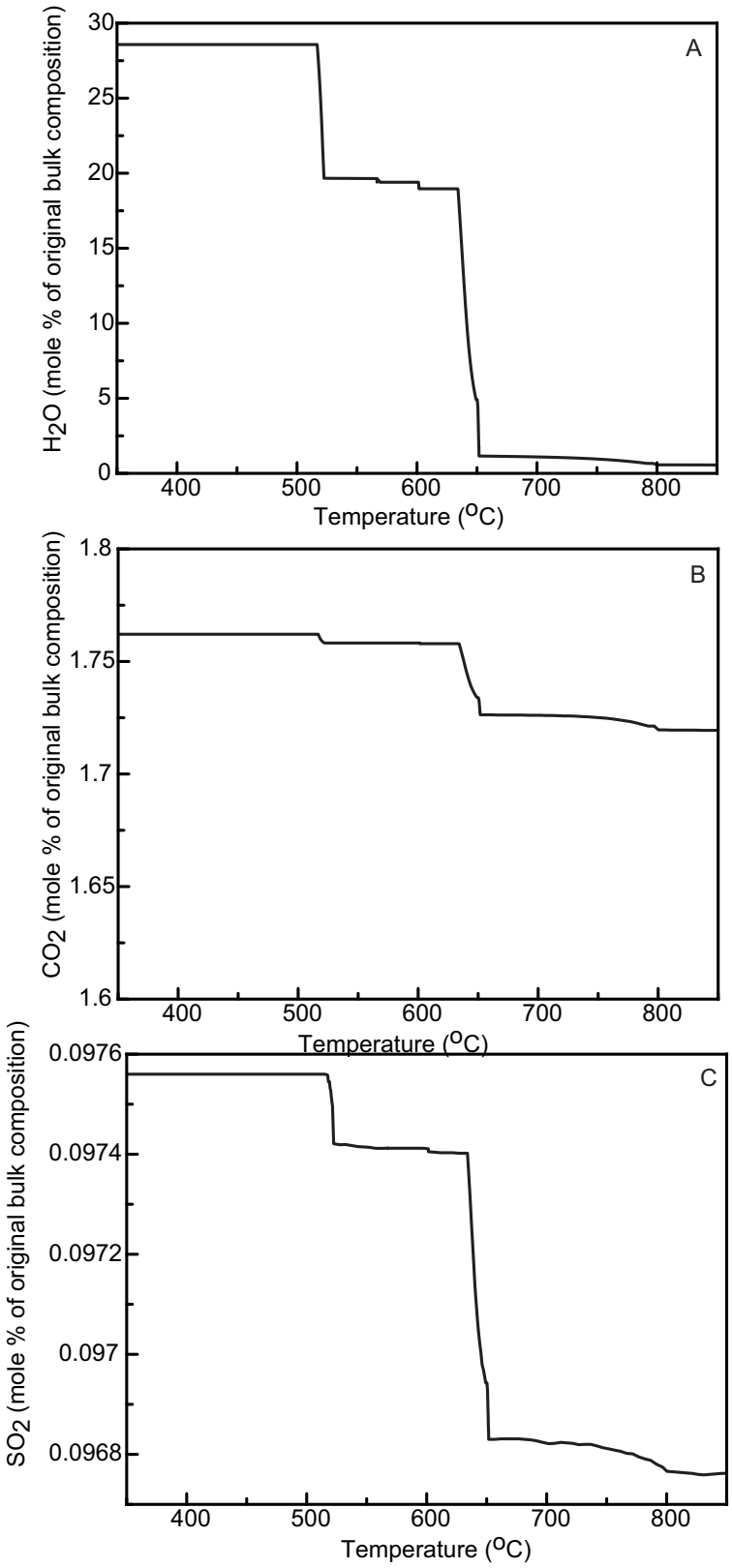
A
H_2O (mole % of original bulk composition)
30
25
20
15
10
5
0
400
500
600
700
800
Temperature (^{O}C)
B
CO_2 (mole % of original bulk composition)
1.8
1.75
1.7
1.65
1.6
400
500
600
700
800
Temperature (^{O}C)
C
SO_2 (mole % of original bulk composition)
0.0976
0.0974
0.0972
0.097
0.0968
400
500
600
700
800
Temperature (^{O}C)

Figure 5:

Figure 6:

Figure 7:

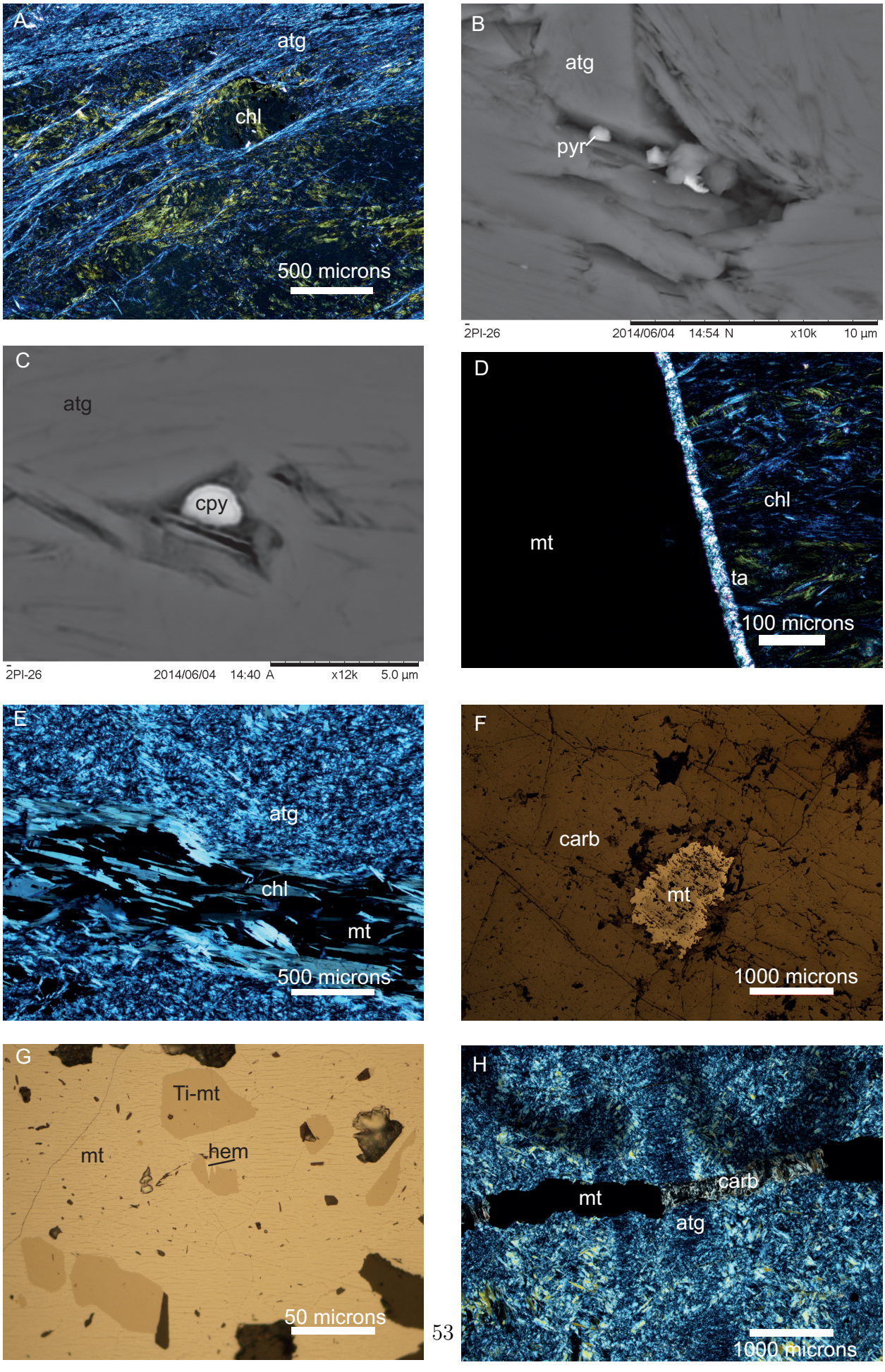
A
atg
chl
500 microns
B
atg
pyr
2PI-26
2014/06/04 14:54 N
x10k
10 µm
C
atg
cpy
2PI-26
2014/06/04 14:40 A
x12k
5.0 µm
D
mt
chl
ta
100 microns
E
atg
chl
mt
500 microns
F
carb
mt
1000 microns
G
Ti-mt
mt
hem
50 microns
H
mt
carb
atg
1000 microns

Figure 8:

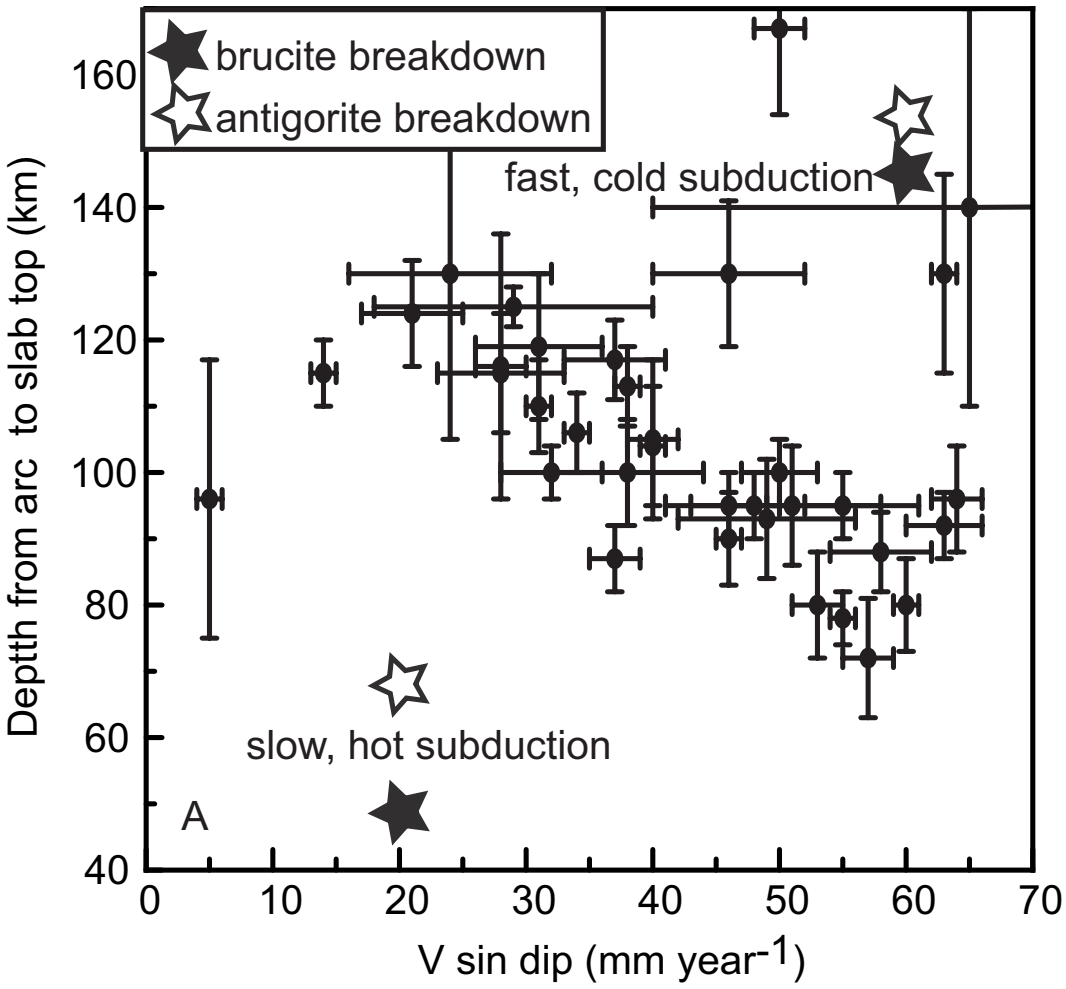
brucite breakdown
antigorite breakdown
fast, cold subduction
slow, hot subduction
A
Depth from arc to slab top (km)
V sin dip (mm year-1)
160
140
120
100
80
60
40
0
10
20
30
40
50
60
70

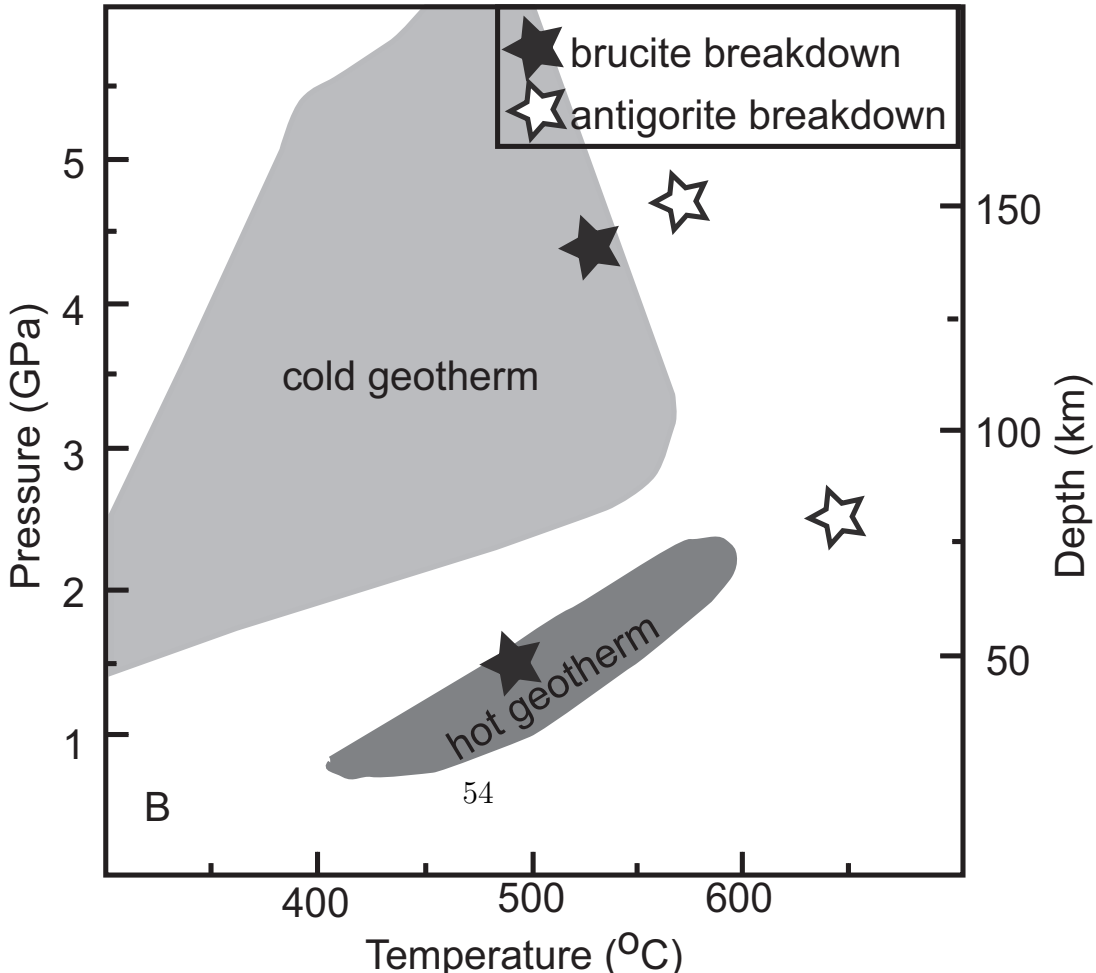
brucite breakdown
antigorite breakdown
cold geotherm
hot geotherm
B
Pressure (GPa)
Depth (km)
Temperature (°C)
5
4
3
2
1
150
100
50
400
500
600